Title: Dynamic changes in the neurogenic potential in the ventricular-subventricular zone of common marmoset during postnatal brain development

Authors

Mariyam Akter[1, 2, #], Naoko Kaneko[1, #, *], Vicente Herranz-Pérez[3, 4], Sayuri Nakamura[1], Hisashi Oishi[5], Jose Manuel García-Verdugo[3], Kazunobu Sawamoto[1, 6, *]

Affiliations

1: Department of Developmental and Regenerative Neurobiology, Institute of Brain Science, Nagoya City University Graduate School of Medical Sciences, 1 Kawasumi, Mizuho-cho, Mizuho-ku, Nagoya, Aichi, 467-8601, Japan

2: Department of Pharmacy, Noakhali Science and Technology University, Noakhali 3814, Bangladesh

3: Laboratory of Comparative Neurobiology, Instituto Cavanilles, Universidad de Valencia, CIBERNED, C/ Catedrático José Beltrán, 2, 46980 Paterna, Valencia, Spain

4: Predepartmental Unit of Medicine, Faculty of Health Sciences, Universitat Jaume I, Av. de Vicent Sos Baynat, 12071 Castelló de la Plana, Spain

5: Department of Comparative and Experimental Medicine, Nagoya City University Graduate School of Medical Sciences, 1 Kawasumi, Mizuho-cho, Mizuho-ku, Nagoya, Aichi, 467-8601, Japan

6: Division of Neural Development and Regeneration, National Institute for Physiological Sciences, 5-1 Higashiyama, Myodaiji, Okazaki, Aichi, 444-8787, Japan

***Corresponding authors**

Kazunobu Sawamoto, Ph.D.

Address: 1 Kawasumi, Mizuho-cho, Mizuho-ku, Nagoya, Aichi, 467-8601, Japan

Telephone number: +81-52-853-8532

Facsimile number: +81-52-851-1898

E-mail: sawamoto@med.nagoya-cu.ac.jp

Naoko Kaneko, M.D., Ph.D.

Address: 1 Kawasumi, Mizuho-cho, Mizuho-ku, Nagoya, Aichi, 467-8601, Japan

Telephone number: +81-52-853-8532

Facsimile number: +81-52-851-1898

E-mail: naokoka@med.nagoya-cu.ac.jp

Running title: Postnatal neurogenesis in common marmosets

Abstract

Even after birth, neuronal production continues in the ventricular-subventricular zone (V-SVZ) and hippocampus in many mammals. The immature new neurons ("neuroblasts") migrate and then mature at their final destination. In humans, neuroblast production and migration toward the neocortex and the olfactory bulb (OB) occur actively only for a few months after birth, and then sharply decline with age. However, the precise spatiotemporal profiles and fates of postnatally born neurons remain unclear due to methodological limitations. We previously found that common marmosets, small non-human primates, share many features of V-SVZ organization with humans. Here, using marmosets injected with thymidine analogue(s) during various postnatal periods, we demonstrated spatiotemporal changes in neurogenesis during development. V-SVZ progenitor proliferation and neuroblast migration toward the OB and neocortex sharply decreased by 4 months, most strikingly in a V-SVZ subregion from which neuroblasts migrated toward the neocortex. Postnatally born neurons matured within a few months in the OB and hippocampus, but remained immature until 6 months in the neocortex. While neurogenic activity was sustained for a month after birth, the distribution and/or differentiation diversity was more restricted in 1-month-born cells than in the neonatal-born population. These findings shed light on distinctive features of postnatal neurogenesis in primates.

Key words: Common marmoset, dentate gyrus, non-human primate, postnatal neurogenesis, ventricular-subventricular zone.

Introduction

After the end of embryonic brain morphogenesis in mammals, most neural stem cells lose their neurogenic properties and differentiate into astrocytes or ependymal cells. However, neuronal production occurs continuously after birth, even in adulthood, in the ventricular-subventricular zone (V-SVZ) located at the lateral walls of the lateral ventricles and in the subgranular zone (SGZ) in the dentate gyrus of the hippocampus. In these areas, neural stem cells with astrocyte-like morphology are maintained to generate rapidly proliferating neuronal progenitors, which produce immature new neurons called neuroblasts (Ihrie RA and A Alvarez-Buylla 2011; Lim DA and A Alvarez-Buylla 2016; Kaneko N *et al*. 2017). The neuroblasts born in the SGZ migrate into the overlying granule cell layer and differentiate into granule cells to contribute to learning and memory function and mood modulation in the hippocampal neuronal circuit (Anacker C and R Hen 2017; Cope EC and E Gould 2019). In contrast, the neuroblasts generated in the V-SVZ make a long journey through the rostral migratory stream (RMS) to the olfactory bulb (OB), where they differentiate into olfactory interneurons within 4 to 6 weeks after they are generated (Lim DA and A Alvarez-Buylla 2016; Lledo PM and M Valley 2016). These adult-born new neurons are known to be involved in odor discrimination and learning (Sakamoto M *et al*. 2014; Lledo PM and M Valley 2016). In addition, after brain injury, V-SVZ-derived neuroblasts migrate toward the injured area to contribute to neuronal regeneration (Lindvall O and Z Kokaia 2015; Kaneko N *et al.* 2017). Therefore, the potential for postnatal neurogenesis and

its manipulation are of great interest to researchers in basic biology and clinical medicine. Advances in our knowledge about the process, regulatory mechanisms and biological significance of postnatal neurogenesis have largely depended on studies using mice, like advances in many other fields of neuroscience.

Humans have a highly developed neocortex and expanded white matter in their large brain, compared with rodents (Zhang K and TJ Sejnowski 2000; Rakic P 2009; Ghosh L and S Jessberger 2013). An additional population of neural progenitor cells, including basal radial glia (or outer radial glia) and intermediate progenitors, in the developing neocortex, contributes to the expansion of the primate neocortex during embryonic morphogenesis (Geschwind DH and P Rakic 2013; Molnar Z *et al*. 2019). Recent studies also revealed several distinct properties of postnatal neurogenesis in the human brain. For example, during the first few months after birth, many proliferating cells and neuroblasts are observed in the V-SVZ adjacent to elongated radial glia-like cells lining the ventricular walls, and then they sharply decline by 6 months, and increasing evidence supports the notion that they disappear before adulthood (Sanai N *et al.* 2011; Dennis CV *et al.* 2016). The adult human V-SVZ has a distinctive three-layer organization (Quinones-Hinojosa A *et al.* 2006). Below a monolayer of multiciliated ependymal cells at the apical surface, two unique layers have been identified: a band of periventricular astrocytes referred to as an astrocytic ribbon, and a hypocellular gap composed of cytoplasmic expansions of ependymal cells and ribbon astrocytes, though their functional significance is still unknown. Interestingly, while a small subpopulation of the V-SVZ-derived neuroblasts migrate into the cortex only during the first few weeks after birth in

rodents (Inta D *et al.* 2008; Le Magueresse C *et al.* 2011), human neonates possess additional migratory paths of neuroblasts directed toward the prefrontal cortex branching from the RMS (Sanai N *et al.* 2011) and toward the cingulate cortex radially from the V-SVZ (Paredes MF *et al.* 2016) for more than a few months. Since these brain regions are highly developed in primates and associated with higher brain functions and also with the etiology/cause of several neuropsychiatric diseases, it is possible that these postnatally generated neuroblasts contribute to the establishment of the elaborate neocortex in humans. However, due to the limited experimental methodology applicable in humans, the time of the birth and the fates of these cells remain to be clarified.

The common marmoset, a New World non-human primate, is well established as a laboratory animal, especially for preclinical studies, due to its relatively small body size and high fecundity. They live in family groups in nature, and show high sociality and cognitive functions (Homman-Ludiye J and JA Bourne 2017). Their brain shares common developmental and structural features with those of other primates, including humans: it contains basal radial glia in the mid-gestation stages and develops a thick neocortical layer (Garcia-Moreno F *et al.* 2012; Kelava I *et al.* 2012), although it lacks complex folding of sulci in the cerebral cortex. We have previously investigated the cellular composition of the V-SVZ in marmosets (Sawamoto K *et al.* 2011). In both neonates and adults, the V-SVZ organization is very similar between marmosets and humans, though the hypocellular gap and astrocytic ribbon in marmosets are thinner than those in humans (Quinones-Hinojosa A *et al.* 2006; Sawamoto K *et al.* 2011). Together, these features indicate that common marmosets

can provide a useful animal model for studying primate postnatal neurogenesis. In this study, using neonatal to adult marmosets with or without injection of thymidine analogues at various time points and for various durations, we demonstrated dynamic changes of the structural and the neurogenic potential in the primate V-SVZ during postnatal development.

Materials and Methods

Animals

Postnatal day (P) 0-3 (*n*=8), 1-month (*n*=11), 2-month (*n*=3), 4-month (*n*=3) and 6-month (*n*=3) common marmosets (*Callithrix jacchus*) obtained from three mating pairs and adult (29- to 34-month) common marmosets (*n*=3) in a domestic animal colony were used. All experiments using live animals were performed in accordance with the guidelines and regulations of Nagoya City University.

BrdU/EdU administration

To label proliferating cells, 5-ethynyl-2'-deoxyuridine [EdU, Abcam, Cambridge, UK, 30 mg/kg, dissolved in sterile phosphate buffered saline (PBS, pH 7.4)] alone or EdU followed by bromodeoxyuridine (BrdU, MilliporeSigma, Burlington, MA, USA, 30 mg/kg, dissolved in sterile PBS), was repeatedly injected into animals intraperitoneally, as shown in Fig. 5A. The equivalent labeling efficiency of the proliferating cells between BrdU and EdU at this dosage and using the detection method described below was confirmed using mice (Supplementary Fig. S1). For short-term fate analyses, EdU was injected once every 2 days

from P1 to P15, or from P31 to P45. For long-term fate analyses, BrdU from P1 to P7 and EdU from P31-P37 were injected three times a day.

Tissue processing

Animals were deeply anesthetized with isoflurane and perfused transcardially with PBS (pH 7.4) followed by 4% paraformaldehyde (PFA) in 0.1 M phosphate buffer (PB, pH 7.4) for immunohistochemistry, or with 2% PFA-2.5% glutaraldehyde in 0.1 M PB for electron microscopy. The brains were extracted and post-fixed for 12 to 48 hours in the same fixative, then cut into 60-µm-thick and 200-µm-thick coronal sections for immunohistochemistry and electron microscopy, respectively, using a vibratome (VT1200S, Leica, Wetzlar, Germany).

Immunohistochemistry

Sections were incubated for 1 hour in blocking solution (10% donkey serum and 0.2% Triton X-100 in PBS) and then for 12 to 48 hours at 4°C with the primary antibody (or antibodies, as indicated in the text). After the sections were washed, they were incubated for 3 h at room temperature with Alexa Fluor-conjugated secondary antibody (1:1,000, Life Technologies, Carlsbad, CA, USA). For signal amplification, the sections were pretreated with 1% H_2O_2 for 1 hour before blocking, and then after incubation with primary antibody (or antibodies, as indicated in the text), the sections were incubated with biotinylated secondary antibody (or antibodies, as indicated in the text) (1:1,000, Jackson Laboratory, Bar Harbor, ME, USA), and treated with the Vectastain Elite ABC kit (Vector Laboratories, Burlingame, CA, USA), and TSA Fluorescence System (PerkinElmer, Waltham, MA, USA). For BrdU staining, sections were treated with 1 M HCl at 64°C for 45 minutes before the H_2O_2 treatment.

The following primary antibodies were used: guinea pig anti-doublecortin (DCX) (1:400, MilliporeSigma), mouse anti-human CD31 (1:100, Agilent, Santa Clara, CA, United States), rabbit anti-myelin basic protein (MBP) (1:400, Abcam), rabbit anti-Ki67 (1:400, Leica), rabbit anti-Mash1 (1:1,000, Abcam), mouse anti-NeuN (1:100, MilliporeSigma), sheep anti-BrdU (1:2,000, Fitzgerald, Acton, MA, USA), and mouse anti-calretinin (1:1,000, MilliporeSigma). For EdU staining, sections were incubated at room temperature with a solution containing 150 mM NaCl, 50 mM Tris buffer (pH 7.5), 2 mM $CuSO_4$(II), 2 μM Alexa Fluor azide (Life Technologies) and 10 mM sodium ascorbate in distilled water for 2 hours and then washed with PBS (Esumi *et al.*, submitted). Cell nuclei were stained with Hoechst 33342 (1:5,000, Life Technologies).

Transmission Electron Microscopy

Sample preparation was performed as described previously (Kaneko N *et al.* 2018). Briefly, 200-μm-thick coronal brain sections were post-fixed with 1% OsO_4 in 0.1 M PB for 2 h, dehydrated with a graded series of alcohol, and embedded in epoxy resin (Durcupan, Fluka Biochemika, Ronkonkoma, NY). Serial semi-thin sections (2.0-μm-thick) were cut with an ultramicrotome (UC7, Leica) using a diamond knife (Histo, Diatome, Hatfield, PA, USA), and stained lightly with 1% toluidine blue. Subsequently, sections cut from selected levels were glued to Durcupan blocks and detached from the glass slide by repeated freezing in liquid nitrogen and thawing. From the semi-thin sections, ultra-thin sections (60-70-nm-thick) were prepared using an ultramicrotome (UC7, Leica) and a diamond knife (SYM2045, Syntek, Kanagawa, Japan), and stained with 2% uranyl acetate for 15 min and with modified

Sato's lead solution for 5 min (Reynolds' solution). Images were captured using a transmission electron microscope (JEM-1400Plus, JEOL, Tokyo, Japan) equipped with a digital camera. Neuroblasts were identified by their electron-dense nucleus and cytoplasm containing abundant microtubules and free ribosomes, whereas astrocytes were identified by their electron-lucent nucleus and cytoplasm and the presence of intermediate filaments and glycogen granules, as previously described (Doetsch F *et al.* 1997; Sawamoto K *et al.* 2011).

Quantification

The absolute number of cells in 60-μm-thick coronal sections from various rostrocaudal levels was counted in a non-blinded manner and then the total number of cells was estimated as the sum of all the counted cells. The numbers of DCX-immunoreactive cells in the V-SVZ, corpus callosum (CC)-neocortex and striatum, and of Ki67-immunoreactive cells in the V-SVZ were counted under an optical microscope (BX-51, Olympus, Tokyo, Japan) with a 20x objective lens. The number of DCX+ cells in the RMS was counted after capturing confocal z-stack images with a step size of 2 μm using a confocal laser microscope LSM700 (Carl Zeiss, Jena, Germany).

To visualize and count double-labeled cells, confocal z-stack images with a step size of 2 μm were captured using a confocal laser microscope LSM700 (Carl Zeiss) with a 20x objective lens. In the cases of the BrdU- and EdU-labeled cells in the neocortex of the 4- and 6-month brain, a 40x objective lens was used. In the neocortex of the 4- and 6-month brain, some of the DCX+ cells were positive for an oligodendrocyte marker, Olig2, and these cells were excluded from the DCX+ cell count. For the analyses of proliferating cells and neuronal

progenitors, cells from five sections were counted, and for the analyses of neuroblasts, cells from three sections were counted. Quantitative data for fate analyses were obtained from one to three sections per analysis.

For quantification of the cell density, the absolute cell number was divided by the area in which the cells were distributed, which was measured using Zen software (Carl Zeiss). For myelin quantification, the average MBP signal intensity in each animal was calculated using confocal images obtained from 3 randomly chosen areas in the CC immunostained for MBP, which was standardized using the average value at 1 month.

To compare the number of neuroblasts in the neocortex at 1 and 2 months, DCX-immunoreactive cells in the comparable column of the neocortex overlying the V-SVZ in one coronal section of each animal were counted. To measure the translocation index, the number of EdU-labeled DCX-immunoreactive cells in the areas over the extension, which includes the CC to the neocortex, was divided by that in the extension.

Statistical Analyses

All data are expressed as the mean ± standard error of the mean (SEM). Normality and equal variances between group samples were assessed using the Shapiro-Wilk test and *F* test, respectively. When normality and equal variance between sample groups were achieved, differences between means were determined by a two-tailed Student's *t* test, paired *t* test, or one-way ANOVA, followed by a Bonferroni test. A *P* value of <0.05 was considered to be statistically significant.

Results

Organization and neuroblast distribution of the V-SVZ during postnatal development

The adult marmoset V-SVZ can be divided in different subregions. It has a large dorsolateral extension between the striatum and the CC (Sawamoto K *et al.* 2011). In this report, we refer to the ventricular wall in this region as the "dorsolateral wall (DW)" and that along the lateral walls lining the main body of the lateral ventricle as the "lateral wall (LW)" (Fig. 1A-B, DW: continuous and broken pink lines; LW: broken cyan lines). The DW is further divided into two subsegments: the narrow area in which the ventricle is collapsed and the opposite two ventricular walls are in contact with each other ("DW-collapsed", continuous pink lines in Fig. 1A'-B), and the wall delineating a small ventricular space containing the cerebrospinal fluid ("DW-open", broken pink lines in Fig. 1A'-B).

We first examined the morphology and distribution of neuroblasts in the V-SVZ at age 1 month using serial coronal brain sections throughout the rostro-caudal levels (Fig. 1A, level I-V) immunostained for a neuroblast marker, DCX (Fig. 1B). The DW was well developed at level II-III, but shrunken at level IV and absent in level V. Since the ventricular collapse was not observed at level I, the DW could not be discriminated from the LW. At levels I and II, DCX+ neuroblasts were accumulated in the ventral part of the LW connected to the RMS, suggesting that their destination was in the OB. We also found a dense accumulation of DCX+ cells in a small area that extended laterally from the dorsal tip of the LW at level I and from the DW-open at level II-IV, which we refer to as the "extension (EX)" (Fig. 1A'-B, red lines).

Using electron microscopy for the analysis of coronal sections corresponding to level III (see diagram in Fig. 1A), we examined the cellular organization of the V-SVZ in each subregion during postnatal development (Fig. 1C-P). As was reported previously (Sawamoto K *et al.* 2011), instead of the typical three-layer organization comprising ependymal, hypocellular gap, and astrocytic ribbon layers seen in the adult animals, the neonatal (0-month) LWs presented a rather thick and pseudo-stratified layer of elongated radial glia-like cells and immature ependymal cells with multiple undeveloped cilia at their apical surface and a very thin (or occasionally no identifiable) hypocellular gap layer (Fig. 1D). The third layer was thick and contained many neuroblasts and astrocytes. In contrast, in the 1-month LW, while ependymal cells still showed elongated columnar morphology, they formed mostly a simple monolayer. The hypocellular gap and astrocytic ribbon were clearly identified (Fig. 1E), more closely resembling the organization of the adult LW (Sawamoto K *et al.* 2011). In spite of these structural differences, we could recognize many neuroblasts throughout the different cell layers (Fig. 1E-F), comparable to those at 0 months.

We further examined the organization of the walls in other areas in the 1-month V-SVZ (Fig. 1G-R, Supplementary Fig. S2). In the striatal side of the DW-open (Fig. 1H-N), the basic layer organization (Fig. 1H-I), as well as the presence of putative neural stem cells projecting an apical expansion with a primary cilium in direct contact with the ventricular surface (type B1 astrocytes, Fig. 1L-N, Supplementary Fig. S2A-B) (Doetsch F *et al.* 1997; Mirzadeh Z *et al.* 2008), were very similar to those in the LW (Fig. 1E-F), though the hypocellular gap was thinner in the DW-open than in the LW (Fig. 1E,H-I). In these areas,

neuroblasts with scant, dark cytoplasm with many free ribosomes and few organelles, microtubule-rich processes and clumped nuclei were frequently integrated into chain-like aggregates (Fig. 1E-F,H-I). They formed short discontinuous adherens junctions and had small free spaces between them (Fig. 1J, inset, filled and open red arrowheads, respectively). The neuroblasts close to the ventricle were surrounded by the expansions from ependymal cells and astrocytes (Fig. 1I), whereas those in the ribbon layer were surrounded by astrocytic cell bodies and processes (Fig. 1F,I,K). Chains of neuroblasts were rarely observed in the upper side of the DW associated with the CC (Fig. 1G). The DW-collapsed typically contained a monolayer of cuboidal ependymal cells, which is typical in the adult LW and undeveloped gap and ribbon layers, and fewer neuroblasts than the LW or DW-open (Supplementary Fig. S2C). Taken together, these features indicate that the transition from the embryonic to adult cellular organization appears to begin soon after birth in the V-SVZ, which can be clearly recognized by 1 month, and the organization of the walls is different among the V-SVZ subregions categorized by their spatial relationships with the ventricle.

In contrast to the ventricular walls, the EX lacked a three-layer organization, and was directly connected with developing CC and the striatum, but not with the ventricle (Fig. 1O-R). Numerous neuroblasts displaying similar ultrastructural features to those in the LW and DW-open were gathered in large clusters (Fig. 1O,P) in which they formed short adherens junctions and had small free spaces between each other (Fig. 1Q, inset, filled and open red arrowheads, respectively). While the chains of neuroblasts in the LW and DW-open of 1-month V-SVZ were isolated from the parenchyma by astrocytes (Fig. 1F,I), similarly to those

in the V-SVZ and RMS of adult rodents (Jankovski A and C Sotelo 1996; Lois C *et al.* 1996; Doetsch F *et al.* 1997) and neonatal humans (Sanai N *et al.* 2011), the large neuroblast clusters in the EX had sparse astrocytic wrapping and frequently contacted non-myelinated axons (Fig. 1R, yellow arrowheads). We also found a huge cluster of neuroblast-like cells in the EX (Supplementary Fig. S2D-F). These cells possessed most of the ultrastructural features of typical neuroblasts contacting each other with short discontinuous junctions (Supplementary Fig. S2E, inset), but had less extensive microtubules (Supplementary Fig. S2E), and occasionally had contacting axons enwrapped by thin myelin sheathes (Supplementary Fig. S2F, purple asterisk). These observations suggest that the mode of migration of the neuroblasts in the EX is different from that in the other regions surrounded by astrocytes.

As electron microscopy observations demonstrated the presence of comparable numbers of neuroblasts in 0-month and 1-month V-SVZ, we further examined the age-dependent changes in the number of neuroblasts at later postnatal periods using brain sections at levels I-V immunostained for DCX (Fig. 2A-F). Since immunostaining for DCX produced weaker signals and stronger background staining in the neonatal brain parenchyma compared with those in brains at older ages, we excluded 0-month animals from this analysis. As expected, the number of DCX+ neuroblasts in the V-SVZ was significantly decreased at 4 and 6 months compared with that at 1 month (Fig. 2B), although it still appeared to be higher than that in adulthood (30-month-old, 81.3 ± 18.7 cells). Chains of neuroblasts became sparse in the LW by 4 months (Fig. 2C). The EX contained many DCX+ neuroblasts, which did not

express oligodendrocyte lineage marker Olig2 at 1 month (Supplementary Fig. S3A-C), and these DCX+ neuroblasts sharply decreased by 6 months and completely disappeared in the adult (30 months of age) (Fig. 2D-E). In contrast, DW-open contained chain-forming neuroblasts at all ages examined, even in adulthood (Fig. 2F) (Sawamoto K *et al.* 2011). Taken together, these findings show that during postnatal development, the distribution of neuroblasts in the V-SVZ is drastically changed in a region-specific manner.

Migration of V-SVZ neuroblasts toward the postnatal brain parenchyma

In the marmoset brain, the RMS arises from the ventral V-SVZ between rostrocaudal level I and II, proceeds ventrally and then turns rostrally toward the OB (Fig. 3A-A'), like the RMSs in other primates (Kornack DR and P Rakic 2001; Pencea V et al. 2001; Bedard A et al. 2002; Curtis MA et al. 2007; Gil-Perotin S et al. 2009; Sanai N *et al.* 2011; Wang C et al. 2011). While neuroblasts are sparsely distributed and do not form chains in the adult marmoset RMS, thick chains of neuroblasts are observed throughout the RMS in neonates (Sawamoto K *et al.* 2011). To understand the changes in neuroblast migration toward the OB during the postnatal brain development, the number of DCX+ neuroblasts in the RMS of the olfactory tract in 1-, 4- and 6-month-old animals was quantified (Fig. 3A-C). The neuroblasts formed chain-like aggregates at all ages until 6 months throughout the three sections examined (Fig. 3B). However, both the area occupied by neuroblasts and the density of neuroblasts in the RMS were significantly decreased with increasing age (Fig. 3C,

Supplementary Fig. S3D), suggesting that addition of new neurons in the OB gradually declines with age.

In the neonatal human brain, neuroblasts in the V-SVZ extensively migrate into the prefrontal cortex and the anterior cingulate cortex during the first few months after birth (Sanai N *et al.* 2011; Paredes MF *et al.* 2016). We investigated whether active migration of neuroblasts into the developing cortex was similarly observed in postnatal marmosets by examining coronal sections at level I-III (Fig. 3D-J), which contained many neuroblasts in the V-SVZ (Fig. 1B). While a neuroblast stream equivalent to the medial migratory stream was absent at all ages, numerous DCX+ neuroblasts were observed in the CC (Fig. 3F) and the deeper cortical layer (layer V-VI, Fig. 3D) at 1 month. These cells co-expressed another neuroblast marker, βIII-tubulin, (Supplementary Fig. S3E). In addition, a few neuroblasts were distributed in the upper cortical layer (layer I-IV, Fig. 3G).

The DCX+ cells in 1-month CC and neocortex had a monopolar or bipolar shape with a long leading process and small oval nucleus, a morphology typical of actively migrating neuroblasts (Fig. 3D,F,G). Notably, neuroblasts extending their process radially toward the cortex were observed in the boundary between the EX and overlying CC (Fig. 3F, arrowheads, Supplementary Fig. S3C), suggesting that some of the neuroblasts in the neocortex are derived from the V-SVZ. Unlike those in the RMS (Fig. 3B), the neuroblasts migrating toward the cortex rarely formed chains or contacted blood vessels (Fig. 3D,J), and they were intimately associated with non-myelinated axons rather than astrocytic processes (Fig. 1P,R).

At 4 and 6 months, the density of DCX+ cells in this region was significantly reduced compared with the density at 1 month (Fig. 3I), and most of the DCX+ cells showed more complex morphologies, with long and branched processes (Fig. 3H), suggesting that they were undergoing differentiation into mature neurons. In young adult animals (30 months old), no DCX+ cells were observed in the neocortex (data not shown). Altogether, these findings indicate that neuroblast migration toward the postnatal neocortex occurs only during the early neonatal period.

We then compared the mode of migration of neuroblasts in the 4-month brain with that in the 1-month brain at a deeper layer of the neocortex (Fig. 3D,E,J). While the percentage of individually migrating cells that were not in contact with blood vessels was significantly lower at 4 months, about 60 % of the neuroblasts were integrated into chains, which were frequently associated with blood vessels (Fig. 3J). We also compared the morphology and distribution of blood vessels, astrocytes, axons and myelin, which might affect neuroblast migration in the CC between 1 month and 4 months (Fig. 3K). There were no significant differences in morphology (Fig. 3D,E) or density of blood vessels (CD31+ area, 1 month, 67397 ± 4881 $\mu m^2/mm^2$; 4 months, 70175 ± 6489 $\mu m^2/mm^2$) or astrocytes (1 month, 440 ± 29.0 cells/mm^2; 4 months, 366 ± 63.4 cells/mm^2). The density of axons visualized by immunostaining of neurofilaments was also not different between these two ages (data not shown). In contrast, while myelin visualized with myelin basic protein (MBP) immunohistochemistry was very sparse in the CC and overlying white matter at 1 month, it was drastically increased at 4 months (Fig. 3K, standardized MBP signal intensity, 1 month,

1.00 ± 0.41; 4 months, 8.23 ± 0.57), suggesting that neuroblasts use vascular scaffolds to pass through the developing myelin toward the cortex.

We also found neuroblasts present in the striatum (Supplementary Fig. S3F-I). They were very sparse at 1 month, sharply increased at 4 and 6 months, and then declined in the adult (Supplementary Fig. S3F-G). Long chains of neuroblasts closely associated with blood vessels were frequently observed in 4- and 6-month striatum (Supplementary Fig. S3F). However, the neuroblasts were mostly distributed in the medial striatum very close to the V-SVZ (Supplementary Fig. S3H-I), and showed migratory morphology at all ages (Supplementary Fig. S3F). Therefore, it is possible that these neuroblasts transiently invade the adjacent striatum during their migration toward the RMS or neocortex, but do not differentiate in the striatum.

Unlike typical migrating neuroblasts in the embryonic brain, V-SVZ-derived neuroblasts possess mitotic potential during their migration in rodent and primate RMS (Pencea V *et al.* 2001; Ikeda M *et al.* 2010; Dennis CV *et al.* 2016). We compared the proliferative activity of the neuroblasts in each area in the V-SVZ and the migration routes (Fig. 3L). While 25.1 ± 0.85%, 23.7 ± 5.09%, 15.5 ± 1.35% and 5.06 ± 1.27% of DCX+ cells in the 1-month LW, DW, EX and RMS co-expressed proliferation marker Ki67, respectively, none of the neuroblasts in the CC or neocortex expressed Ki67. Moreover, neuroblasts in the striatum did not express Ki67 at any age. These observations suggest that the mitotic potential can be retained in the V-SVZ-derived neuroblasts migrating toward the OB, but not those migrating in the neocortex or striatum.

Taken together, our findings indicate that V-SVZ-derived neuroblasts show distinct time-windows for their active migration, migration mode and mitotic capacity depending on their destination, namely, the OB or neocortex in the postnatal primate brain.

Spatiotemporal differences in proliferation activity in the postnatal V-SVZ

As the organization and neuroblast distribution are different between different areas in the V-SVZ (Fig. 1,2), and the neuroblasts have different migration routes depending on age (Fig. 3), we next compared cell proliferation activities among these areas and at different ages. Although previous studies focused on the rostral V-SVZ for analyzing postnatal neurogenesis, we found a non-negligible number of Ki67+ proliferating cells in the caudal V-SVZ (Supplementary Fig. S4 A,B). Therefore, we evaluated the neurogenic activity of the LW, DW and EX using coronal sections of the postnatal animals immunostained for proliferation marker Ki67 and/or transit amplifying neuronal progenitor marker Mash1 throughout rostrocaudal levels I-V (Fig. 4A-C, Supplementary Fig. S4A-C). At 0 and 1 month, more than 50% of the Ki67+ cells were positive for Mash1, indicating the high neurogenic potential of the early-postnatal marmoset V-SVZ. The number of Ki67+ cells was significantly increased at LW from 0 to 1 month, and then decreased by 4 months (Fig. 4A,D). The decline in Ki67+ cells after 1 month was more drastic in the EX (Fig. 4B,D). In the adult brain, Ki67+ cells were located only in the LW and DW (30 months, 32.3 ± 3.8 cells). These age-dependent changes were similar to the changes in the number of Ki67+Mash1+ cells (Fig. 4C,E, Supplementary Fig. S4C), although we did not find

statistically significant differences due to the limited sample size. Notably, in the EX, we found dense accumulation of Ki67+Mash1+ cells at 0 and 1 month (Fig. 4C), which decreased sharply by 4 months and completely disappeared in the adult (Fig. 4E, Supplementary Fig. S4C), suggesting that EX is involved in the production of neuroblasts only during the early postnatal period.

Interestingly, no obvious age-dependent change in cell proliferation was observed in the DW (Fig. 4D,E). We therefore compared the density of Ki67+Mash1+ cells in each subregion of the V-SVZ. The Ki67+Mash1+ cell density was similar among the LW, DW and EX at 0 and 1 month (Fig. 4F,G); however, it tended to be higher in the DW than in the other regions at 4 months (Fig. 4E), suggesting that the DW retains neurogenic potential longer than the other areas after birth.

Taken together, our findings show that while high neurogenic activity is maintained throughout the V-SVZ for more than a month after birth, it declines with age in a region-specific manner in the postnatal marmoset brain.

The fate of postnatally born neurons in the olfactory bulb

In the postnatal rodent brain, after reaching the OB, the majority of the neuroblasts born in the V-SVZ differentiate into granule cells, olfactory interneurons in the granule cell layer, within 4 weeks, while about 10% of them differentiate into periglomerular cells, another type of interneuron, in the glomerular layer within 6 weeks (Lois C and A Alvarez-Buylla 1994; Petreanu L and A Alvarez-Buylla 2002; Carleton A *et al.* 2003; Hack MA *et al.*

2005; Merkle FT *et al.* 2007). In common marmosets, as the cell proliferation activity in the V-SVZ was not decreased within the first month after birth (Fig. 4), the animals were injected with thymidine analogue EdU every 2 days from P1 to P15 and from P31 to P45, and then fixed at P30 (1 month) and P60 (2 months), respectively (Fig. 5A). In spite of the extensive labeling of newly generated cells, the vast majority of EdU+ cells in the OB were co-labeled with DCX, but not with NeuN (Fig. 5B-D), indicating that they need more than 1 month to mature in the marmoset OB during postnatal development, similarly to those in the adults. To trace the longer-range fate of the postnatally born cells, marmosets injected with BrdU three times a day from P1 to P7, followed by EdU injection from P31 to P37, were fixed at 4 or 6 months of age (Fig. 5A, E-K). A large number of BrdU-labeled neonatal-born and EdU-labeled 1-month-born cells that expressed NeuN (BrdU+NeuN+ and EdU+NeuN+, respectively) were observed both in the 4- and 6-month OBs (Fig. 5F-G), but none of the BrdU- or EdU-labeled cells expressed DCX (Fig. 5E). These data suggest that, while some of the neuroblasts might be eliminated by cell death in the OB, as reported in rodents (Yamaguchi M and K Mori 2005; Kato Y *et al.* 2012), surviving neuroblasts mature into neurons within 3 to 4 months in the marmoset OB during postnatal development. Although the size of the OB was closely comparable at birth and 1 month (data not shown), the density of neonatal-born and 1-month-born neurons was reduced by about 43% and 65%, respectively, from 4 months to 6 months of age (Fig. 5G), suggesting that postnatally born neurons are extensively eliminated after maturation.

Previous studies using rodents revealed that the final positioning of new granule cells differs according to animal age: neonatal-born cells are mainly distributed in the outer granule cell layer, whereas adult-born cells reside in the inner granule cell layer (Lemasson M *et al.* 2005). We examined the final destination of the BrdU- and EdU-labeled cells in the 6-month marmoset OB. In both the neonatal-born (BrdU+) and 1-month-born (EdU+) populations, the majority (about 60%) of labeled neurons were distributed in the outer granule cell layer, which was similar to the proportion of neonatal-born neurons in the mouse OB (Fig. 5H). However, notably, while about 11% of neonatal-born neurons resided in the glomerular layer, very few 1-month-born neurons were observed there (Fig. 5I). These results imply that production of periglomerular cells is restricted to the early postnatal period in the primate brain, which is in clear contrast to the production of periglomerular cells in rodents, in which 10% of newly generated neurons are differentiated into periglomerular cells continuously even in adulthood (Hack MA *et al.* 2005; Bragado Alonso S *et al.* 2019).

Olfactory interneurons are classified according to their expression of mutually exclusive chemical markers (Kosaka T and K Kosaka 2016), and production of each neuronal subtype is temporally and spatially regulated in the postnatal brain (Merkle FT *et al.* 2007; Young KM *et al.* 2007; Batista-Brito R *et al.* 2008; Merkle FT *et al.* 2014). We investigated the expression of calretinin, a chemical marker for an olfactory granule cell subtype, in the postnatally born neurons in the 6-month granule cell layer in marmosets. The percentage of calretinin-expressing cells was significantly higher in 1-month-born cells than in neonatal-born cells (Fig. 5J-K). Therefore, while the number and survival rate of olfactory

interneurons are very similar between the neonatal-born and 1-month-born populations, the final destination and differentiation of these two populations are distinctive, suggesting that the V-SVZ at 0 month and that at 1 month play different roles in postnatal development of the OB in this primate.

The fate of postnatally born neurons in the neocortex

Although a previous study revealed extensive migration of neuroblasts from the neuroblast pool adjacent to the lateral ventricle toward the neocortex in human neonates (Paredes MF *et al.* 2016), their birthdate and long-term fates were unknown due to technical limitations. Since our results suggest the presence of V-SVZ neuroblasts migrating toward the neocortex in early postnatal marmoset brains (Fig. 3), we investigated the fates of postnatal-born cells in the neocortex using brain sections injected with EdU, or BrdU followed by EdU, at different postnatal periods (Fig. 5A, L-U). The density of DCX+ cells distributed in the CC-neocortex was not significantly different between 1-month and 2-month animals treated with EdU from P1 to P15 and from P31 to P45, respectively (Fig. 5N, Supplementary Fig. S5): in these animals, more than 20% of the DCX+ cells in the EX and the CC-neocortex were labeled with EdU (Fig. 5L,M,O). The neonatal-born and 1-month-born EdU+DCX+ cells in the neocortex showed simple migratory morphology (Fig. 5L,M), similar to the morphology of the EdU-negative neuroblasts surrounding these neonatal-born and 1-month-born EdU+DCX+ cells in the same regions. The translocation index represented by the ratio of the number of EdU+DCX+ cells in the CC-neocortex to that in the EX in a

vertical column was not significantly different between 1 month and 2 months (Fig. 5P), suggesting that migration of the neonatal-born and 1-month-born neuroblasts from the V-SVZ toward the neocortex occurred with similar efficiency in the following month.

Next, we examined the long-term fate of the neonatal-born (BrdU+) and 1-month born (EdU+) neuroblasts in the 4-month and 6-month neocortex. While a small fraction of the neonatal-born and 1-month-born cells in the deeper layers had migratory morphology, the majority of them throughout the cortical layers had a large round nucleus and multiple DCX+ processes (Fig. 5Q,R), suggesting that these cells were not migrating but were undergoing maturation, as were the surrounding neuroblasts without labeling (data not shown).

While the DCX+ multipolar cells did not express astrocytic (S100β) or microglial (Iba1) markers (Supplementary Fig. S6A-C), some of them expressed oligodendrocyte lineage marker Olig2 in the 4- and 6-month neocortex. In this paper, we only focused on the DCX+ cells that did not express Olig2 (Supplementary Fig. S6D). Notably, the density of 1-month-born neuroblasts was much lower than that of neonatal-born neuroblasts in both 4-month and 6-month neocortex (Fig. 5T), although the difference did not reach statistical significance due to the limited sample size. Unlike the new neurons in the OB (Fig. 5G), the density of these postnatally born neuroblasts was not significantly reduced in the neocortex between the age of 4 months and 6 months (Fig. 5T). Given that the densities of neonatal-born and 1-month-born neuroblasts in the 1- and 2-month neocortices, respectively, were comparable (Fig. 5N), 1-month-born neuroblasts were more extensively eliminated during the third and fourth months. Moreover, only a few BrdU+ cells, and no EdU+ cells, were

found to be positive for NeuN (Fig. 5S) or GABAergic neuron marker GABA (Supplementary Fig. S6E-F) at 4 and 6 months.

During cortical morphogenesis in the embryonic brain, the positioning of neurons is determined by their birthdate (Lim L *et al.* 2018; Silva CG *et al.* 2019). Neuroblast migration toward the cortex has also been reported in neonatal mice and primates; however, it is not known how the positioning of these neuroblasts is regulated. We compared the distribution of neonatal-born and 1-month-born DCX+ differentiating neuroblasts in the 6-month neocortical layers. While neonatal-born neurons were distributed almost uniformly throughout the layers, 1-month-born cells were rather accumulated in the deeper layers. The percentage of thymidine analogue-labeled neuroblasts residing in the deeper layer was significantly higher in the 1-month-born group than in the neonatal-born group (Fig. 5U).

Taken together, these facts support the notion that while neonatal-born and 1-month-born neuroblasts migrate extensively toward the neocortex, their final destination, survival rate and maturation potential are altered depending on their birthdate, and all of these are more limited in 1-month-born cells than in neonatal-born cells.

The fate of postnatally born neurons in the striatum

At 1 month, neuroblasts were very sparsely observed in the striatum, and none of them were labeled with EdU that had been injected at P1-15 (Supplementary Fig. S6E,G). At 2 months, the number of neuroblasts was increased, and some of them were labeled with EdU injected at P31-45 (Supplementary Fig. S6H). Although there were many DCX+ neuroblasts

in the 6-month striatum close to the V-SVZ (Supplementary Fig. S3F-G), we did not detect any BrdU-labeled neonatal-born (data not shown) or EdU-labeled 1-month-born cells expressing DCX (Supplementary Fig. S6I) or NeuN (data not shown). Therefore, at least a fraction of the neuroblasts observed in the striatum during the later postnatal period were generated postnatally, possibly in the V-SVZ (based on their distribution pattern showing that they were accumulated in the medial striatum close to the V-SVZ) (Supplementary Fig. S3H-I). However, they did not stay or differentiate inside the striatum.

Hippocampal neurogenesis during postnatal development

In addition to the V-SVZ, the hippocampal dentate gyrus contains neural progenitor cells that can generate neuroblasts throughout life in many mammals (Anacker C and R Hen 2017). A previous study revealed that new neurons need about 6 months to mature in the dentate gyrus in adult non-human primates (Kohler SJ *et al.* 2011). We first examined the cell-proliferation activity in the subgranular zone, where the hippocampal neural stem/progenitor cells reside at 0 and 1 month, and found that there were no significant differences between these two ages (Fig. 6A-B). We examined the birthdate-dependent difference in the fate of postnatally born new neurons in the developing hippocampus using animals injected with EdU alone (P1-P15 or P 31-P45) or BrdU (P1-P7) followed by EdU (P31-P37) (Fig. 5A). In the animals fixed at 1 month and 2 months following EdU injection from P1 to P15 and P31 to P45, respectively, most of the EdU-labeled cells in the granule cell layer and subgranular zone expressed DCX, but not NeuN (Fig. 6C). In contrast, in the 4- and 6-month animals (Fig. 6D-H), most of the

neonatal-born (BrdU+) and 1-month-born (EdU+) cells were distributed in the granule cell layer, and generally expressed NeuN (Fig. 6D-E'), but rarely expressed DCX (data not shown), suggesting that the postnatally born cells differentiate into neurons by 4 months. The density of 1-month-born neurons tended to be higher than that of 0-month-born cells at 4 months, and was significantly higher at 6 months (Fig. 6G), while the densities of both of them were not significantly altered between 4 and 6 months. There results suggest that both neonatal-born and 1-month-born cells efficiently contribute to postnatal neurogenesis in the dentate gyrus, unlike those in the neocortex.

In rodents, new neurons generated in the embryonic and early postnatal periods are mainly distributed in the outer granule cell layer, whereas adult-born neurons are distributed in the inner layer (Kempermann G *et al.* 2003; Mathews EA *et al.* 2010). We investigated whether such birthdate-dependent distribution patterns were also observed in the neonatal-born and 1-month-born neurons in common marmosets. In the marmoset granule cell layer, while granule cells are densely aligned in the inner and medial layers, similarly to the granule cells in rodents, they are sparsely distributed in the outer layer (Fig. 6D, oGCL). Regardless of their locations in the granule cell layer, the vast majority of these cells expressed dentate granule cell marker Prox1 (Supplementary Fig. S7). Neonatal-born (BrdU+) neurons were distributed widely from the inner to outer layers of the granule cell layer (Fig. 6D,H). In addition, some of the neonatal-born neurons were located below the granule cell layer in the subgranular zone and the hilus (Fig. 6F,H). On the other hand, 1-month-born (EdU+) neurons were accumulated in the inner to medial granule cell layers (Fig. 6D,H). Although the

function of new neurons in the hilus is currently unknown, our findings suggested that the fate of postnatally born neurons was birthdate dependent, as was the fate of those derived from the V-SVZ.

Discussion

Previous studies suggested that neurogenic potential is high just after birth, then sharply declines with age and almost disappears in adulthood in primates, including humans (Leuner B *et al.* 2007; Sanai N *et al.* 2011; Dennis CV *et al.* 2016; Sorrells SF *et al.* 2018). However, its precise spatiotemporal profile and the fates of the postnatally born neurons have not been investigated. In this study, using common marmosets injected with thymidine analogues during different postnatal periods, we obtained a detailed profile of the age-dependent changes in the organization and neurogenic potential in the V-SVZ (Fig. 1-5) and the hippocampus (Fig. 6) and clarified the diverse fates of the postnatally born neurons depending on their birthdate and destination during postnatal development.

In common marmosets, the proliferative activity of neuronal progenitors in the V-SVZ was sustained during the first month after birth, and then decreased drastically to levels close to those in the adult animals by 6 months of age (Fig. 4). These temporal profiles are well consistent with those in human infants (Sanai N *et al.* 2011; Dennis CV *et al.* 2016). In spite of the comparable proliferative activity, electron microscopic observation of the V-SVZ organization revealed clear structural differences between neonates and marmosets at 1 month of age. Whereas the neonatal V-SVZ contained many radial glia (putative neural

stem/progenitor cells in the late phase of embryonic brain morphogenesis) by 1 month of age, the three-layer organization of the V-SVZ, a unique cellular composition in adult humans (Sanai N *et al.* 2004; Quinones-Hinojosa A *et al.* 2006) and non-human primates, including marmosets (Gil-Perotin S *et al.* 2009; Sawamoto K *et al.* 2011), had already developed at 1 month (Fig. 1). Interestingly, while both the neonatal-born and 1-month-born neuroblasts migrated toward the OB and the neocortex to similar extents, our BrdU/EdU-mediated fate-mapping study showed that the final distribution, differentiation and survival were significantly different between these two populations. In the OB, neonatal-born cells, but not 1-month-born cells, were distributed in the glomerular layer in addition to the granule cell layer (Fig. 5H-I). Moreover, in the neocortex, while the neonatal-born neuroblasts were distributed throughout the layers, most of the 1-month-born neuroblasts were localized in the deeper layers (Fig. 5U). Therefore, although proliferation activity of the progenitors in the V-SVZ is sustained for 1 month after birth, the diversity of the fates of their progeny decreases rapidly during the early postnatal period.

Previous studies using rodents demonstrated revealed the migration and maturation processes of the new neurons in the postnatal OB in detail and demonstrated the involvement of these neurons in odor discrimination and olfactory learning (Ihrie RA and A Alvarez-Buylla 2011; Lim DA and A Alvarez-Buylla 2016; Lledo PM and M Valley 2016; Kaneko N *et al.* 2017). On the other hand, while we and others have previously reported that there were no BrdU+ cells expressing mature neuronal marker NeuN in the OB 1 month after BrdU injection in adult macaques, squirrel monkeys and common marmosets (Kornack DR and P

Rakic 2001; Bedard A *et al.* 2002; Sawamoto K *et al.* 2011), long-term fates of neuroblasts in the OB have not been investigated in primates. In common marmosets during postnatal development, new neurons need about 3 months to mature in the OB (Fig. 5) , which is about twice as long as needed in rodents (Petreanu L and A Alvarez-Buylla 2002; Carleton A *et al.* 2003). Periglomerular cells are a subtype of interneurons that reside in the glomerular layer of the OB, and that are directly involved in the input of olfactory stimulation into the bulbs. In rodents, while about 10% of newly added neurons differentiate into periglomerular cells continuously in adulthood (Lois C and A Alvarez-Buylla 1994; Hack MA *et al.* 2005), our results indicate that periglomerular cells are produced only in the neonatal V-SVZ in common marmosets. We found that, among the granule cells, calretinin-expressing cells were more actively produced at age 1 month than in neonates (Fig. 5). Calretinin+ granule cells are involved in complex odor discrimination tasks in rodents (Hardy D *et al.* 2018), and their production reaches a peak in the early neonatal period in mice (Batista-Brito R *et al.* 2008). Taken together, these facts show that although olfactory neurogenesis is active during postnatal development in primates, the temporal profile of the production of interneuron subtypes is notably different between rodents and primates. Currently, the exact roles of each interneuron subtype are largely unknown even in mice, and it is difficult to compare the odor discrimination ability among species (Wackermannova M *et al.* 2016); however, these differences found in the present study might reflect different roles of postnatal neurogenesis in the development and/or regulation of olfaction between the species.

We found that the proliferative activity of the neuronal progenitor cells and its age-dependent decrease varied among the LW, DW and EX regions, which have different spatial relationships with the lateral ventricles in the V-SVZ. While cell proliferation in the EX was drastically reduced at all ages examined after 1 month (Fig. 4) in synchrony with a decrease of the number of neuroblasts migrating toward the neocortex (Fig. 3), these cell activities and numbers were maintained in the DW for over 6 months (Fig. 4). In addition, chains of neuroblasts and proliferating cells were observed almost exclusively in the DW-open in the adult V-SVZ (Fig. 2) (Sawamoto K *et al.* 2011). These observations suggest that stem cells in these regions are differently affected by age.

Using labeling techniques that are highly area-specific, it has been verified that the postnatal stem cells in different regions of the V-SVZ produce different types of neurons in mice (Merkle FT *et al.* 2007; Young KM *et al.* 2007; Batista-Brito R *et al.* 2008; Merkle FT *et al.* 2014). In addition, a previous study using immunohistochemistry showed distinct region-specific expression patterns of several transcription factors in adult common marmoset V-SVZ cells (Azim K *et al.* 2013). Therefore, the different fates of the newly generated cells according to their birthdate (Fig. 5) are thought to be attributable to differences in the timing of activation of stem cell subpopulations.

While human brains are characterized by their thick and highly gyrified neocortex, common marmoset brains are lissencephalic. Using serial sections of the 1-month brain, we found that marmosets do not have an additional migratory stream leading to the prefrontal cortex, unlike human neonates, in which neuroblasts migrate in a stream branching off the

proximal limb of the RMS toward the prefrontal cortex (Sanai N *et al.* 2011). However, unexpectedly, the temporal profile of marmoset V-SVZ-derived neuroblast migration toward the overlying neocortex was very similar to the corresponding profile in humans (Paredes MF *et al.* 2016): neuroblasts with migratory morphology are abundantly observed during the first 2 months, but sharply decline by 6 months, and disappear by 2 years of age (Paredes MF *et al.* 2016) (Fig. 3). Neuroblasts migrating in the neonatal human neocortex were suggested to be derived from the embryonic ganglionic eminence based on their postmitotic properties and expression of transcription factors associated with this region. By repeated labeling with thymidine analogues, we demonstrated that over 20% of the neuroblasts in the neocortex were born in the postnatal brain (Fig. 5O). This proportion might be an underestimate, as our labeling methods could not label all of the newborn cells due to the rapid clearance of thymidine analogues from the circulation.

Therefore, though methodological limitations to labeling newly generated cells prevent further studies of postnatal neurogenesis in humans, it is possible that the postnatal human V-SVZ also generates neuroblasts destined for the neocortex. Human infants have accumulations of postmitotic neuroblasts forming a distinct arch-shaped structure, referred to as an “arch”, adjacent to the anterior body of the lateral ventricle and within the neighboring subcortical white matter (Paredes MF *et al.* 2016). We found the EX in early postnatal marmosets, which contained many neuroblasts, some of which were ready to migrate toward the neocortex (Fig. 3). While the neuroblasts starting radial migration toward the neocortex were postmitotic, the EX contained many proliferating neuronal progenitors as well as

neuroblasts, unlike the arch (Fig. 4). Interestingly, arch-like organization is also observed in ferrets, which possess a gyrified cortex (Ellis JK *et al.* 2019), suggesting that the presence of an arch is associated with cortical gyrification rather than evolutionary similarity with humans.

In adult mouse brains, neuroblasts in the V-SVZ and the RMS are integrated in a chain surrounded by astrocytic tunnels (Jankovski A and C Sotelo 1996; Lois C *et al.* 1996) that control their migration (Bolteus AJ and A Bordey 2004; Snapyan M *et al.* 2009; Garcia-Marques J *et al.* 2010; Kaneko N *et al.* 2010), and are occasionally observed migrating along blood vessels (Snapyan M *et al.* 2009; Kojima T *et al.* 2010). Although the blood vessels provide several factors that regulate neuroblast migration (Kaneko N *et al.* 2017), their role as a scaffold appears not to be essential for these migratory pathways toward the OB, given that only a small population of the neuroblasts contacts blood vessels. On the other hand, we previously found that neuroblast migration toward an injured area is highly dependent on the vascular scaffold in the post-stroke striatum (Yamashita T *et al.* 2006; Kojima T *et al.* 2010; Fujioka T *et al.* 2017), where injury-activated astrocytes inhibit their migration (Kaneko N *et al.* 2018). Therefore, neuroblasts might need vascular scaffolds for their migration in a non-permissive microenvironment. In marmosets, the neuroblasts migrating toward the neocortex in the 1-month brain were individual cells, and independent of the blood vessels (Fig. 3). Close observation under the electron microscope revealed that the plasma membranes of these cells were making direct contact with non-myelinated axons rather than astrocytes (Fig. 1). By 4 months, the number of neuroblasts distributed in these areas was drastically reduced

(Fig. 3), which might have been due to the rapid promotion of axonal myelination in the CC, since myelin-associated proteins are reported to suppress neuronal migration (Mathis C *et al.* 2010; Yu S *et al.* 2016) as well as neurite extension (Schwab ME 2010). About 40% of these neuroblasts were localized along blood vessels, frequently forming chains among the myelinated axons in the developed CC and the cortex (Fig. 3K). Intimate association of neuroblasts with blood vessels is also observed in the middle layer of the arch in humans (Paredes MF *et al.* 2016). Therefore, blood vessels might provide an efficient scaffold for the long-distance migration of the V-SVZ-derived neuroblasts in non-permissive microenvironments in the primate brain.

In human infants, DCX+ cells in the anterior cingulate cortex express GABAergic neuron marker GAD67 and interneuron markers including calretinin, neuropeptide Y, somatostatin or calbindin, and these cells are considered to mature and reside there during the first 5 months after birth (Paredes MF *et al.* 2016), although fate mapping studies cannot be performed in humans. In the marmoset brain, while both BrdU-labeled neonatal-born and EdU-labeled 1-month-born neuroblasts migrating into the OB and hippocampal granule cell layer expressed NeuN by 4 months, the vast majority of them in the neocortex expressed DCX even at 6 months (Fig. 5). They developed multiple neurites and sometimes expressed interneuron marker calretinin, suggesting that they were undergoing differentiation. However, we could find only a small number of neonatal-born cells (Fig. 5S), and no 1-month-born cells, that expressed NeuN, and none of the labeled cells expressed other interneuron markers except for GABA (Supplementary Fig. S6F) in the animals at either 4 or 6 months of age.

Since DCX+ cells are not observed in the young adult (30-month-old) neocortex, the DCX+ postnatal-born cells might mature or die by that age. Though it is possible that the postnatal-born DCX+ cells with differentiating morphology play some role in the cortical neuronal circuit, these results suggest a limited contribution of the postnatally born cells to cortical development, at least under physiological conditions in common marmosets. It will be interesting to study whether these cells mature to compensate for the function of lost neurons after brain injury, as we have recently reported in mice (Jinnou H *et al.* 2018).

Although the possible occurrence of neurogenesis in the postnatal human hippocampus is of great interest and under debate among researchers (Paredes MF *et al.* 2018; Parolisi R *et al*. 2018; Duque A and R Spector 2019), further technological developments that will overcome current methodological limitations are needed to address the issue. Non-human primate studies can provide information useful for understanding the human brain. In this report, we demonstrated spatiotemporal profiles of the organization and neurogenic activity of the V-SVZ during postnatal development in common marmosets, which share much in common with those in human infants. By thymidine analogue injection at different time points and for different durations, here we revealed for the first time the fate of the postnatally born cells in detail in the brain of a non-human primate. These findings shed light on the capacity and limitations of endogenous neurogenesis in the primate brain.

Funding

This study was supported by research grants from Japan Society for the Promotion of Science KAKENHI (17H01392, 17H05750, 19H04757, 19H04785, 18KK0213 [to K.S.], 17K07114 [to N.K.]), Program for Advancing Strategic International Networks to Accelerate the Circulation of Talented Researchers (S2704 [to N.K., V.H-P., J.M.G-V., and K.S.]), Bilateral Open Partnership Joint Research Projects (to K.S.), Japan Agency for Medical Research and Development (JP19bm0704033, JP19gm1210007 [to K.S.], JP18jm0210060 [to N.K., and K.S.]), Spanish Ministry of Science, Innovation and Universities (PCI2018-093062 [to V.H-P. and J.M.G-V.]), Spain Cell Therapy Network (TerCel-RD16/0011/0026 to J.M.G-V.), Grant-in-Aid for Research at Nagoya City University (to K.S.), the Canon Foundation (to K.S.), the Mitsubishi Foundation (to K.S.), the Uehara Memorial Foundation (to K.S.) and the Takeda Science Foundation (to N.K. and K.S).

Acknowledgements

We thank Mr. Yukio Wakimoto and Mr. Masayuki Nishio (Nagoya City University), and Dr. Ichiro Miyoshi (Tohoku University, Japan) for supporting animal care and Dr. Shigeyuki Esumi (Kumamoto University, Japan), Ms. Heeju Pae (Nagoya City University) and Mr. Kwon In Beom (Hanyang University, Korea) for technical support.

Author contributions

M.A., N.K. and K.S. designed research. M.A., N.K., S.N., and H.O. performed animal experiments. N.K., V.H-P., and J.M.G-V. performed electron microscopy. M.A., N.K., and K.S. wrote the manuscript.

Corresponding authors

Kazunobu Sawamoto, Ph.D.

Address: 1 Kawasumi, Mizuho-cho, Mizuho-ku, Nagoya, Aichi, 467-8601, Japan

Telephone number: +81-52-853-8532

Facsimile number: +81-52-851-1898

E-mail: sawamoto@med.nagoya-cu.ac.jp

Naoko Kaneko, M.D., Ph.D.

Address: 1 Kawasumi, Mizuho-cho, Mizuho-ku, Nagoya, Aichi, 467-8601, Japan

Telephone number: +81-52-853-8532

Facsimile number: +81-52-851-1898

E-mail: naokoka@med.nagoya-cu.ac.jp

References

Anacker C, Hen R. 2017. Adult hippocampal neurogenesis and cognitive flexibility - linking memory and mood. Nature reviews Neuroscience. 18:335-346.

Azim K, Zweifel S, Klaus F, Yoshikawa K, Amrein I, Raineteau O. 2013. Early decline in progenitor diversity in the marmoset lateral ventricle. Cerebral cortex. 23:922-931.

Batista-Brito R, Close J, Machold R, Fishell G. 2008. The distinct temporal origins of olfactory bulb interneuron subtypes. The Journal of neuroscience : the official journal of the Society for Neuroscience. 28:3966-3975.

Bedard A, Levesque M, Bernier PJ, Parent A. 2002. The rostral migratory stream in adult squirrel monkeys: contribution of new neurons to the olfactory tubercle and involvement of the antiapoptotic protein Bcl-2. The European journal of neuroscience. 16:1917-1924.

Bolteus AJ, Bordey A. 2004. GABA release and uptake regulate neuronal precursor migration in the postnatal subventricular zone. The Journal of neuroscience : the official journal of the Society for Neuroscience. 24:7623-7631.

Bragado Alonso S, Reinert JK, Marichal N, Massalini S, Berninger B, Kuner T, Calegari F. 2019. An increase in neural stem cells and olfactory bulb adult neurogenesis improves discrimination of highly similar odorants. The EMBO journal. 38.

Carleton A, Petreanu LT, Lansford R, Alvarez-Buylla A, Lledo PM. 2003. Becoming a new neuron in the adult olfactory bulb. Nature neuroscience. 6:507-518.

Cope EC, Gould E. 2019. Adult Neurogenesis, Glia, and the Extracellular Matrix. Cell stem cell. 24:690-705.

Curtis MA, Kam M, Nannmark U, Anderson MF, Axell MZ, Wikkelso C, Holtas S, van Roon-Mom WM, Bjork-Eriksson T, Nordborg C, Frisen J, Dragunow M, Faull RL, Eriksson PS. 2007. Human neuroblasts migrate to the olfactory bulb via a lateral ventricular extension. Science. 315:1243-1249.

Dennis CV, Suh LS, Rodriguez ML, Kril JJ, Sutherland GT. 2016. Human adult neurogenesis across the ages: An immunohistochemical study. Neuropathology and applied neurobiology. 42:621-638.

Doetsch F, Garcia-Verdugo JM, Alvarez-Buylla A. 1997. Cellular composition and three-dimensional organization of the subventricular germinal zone in the adult mammalian brain. The Journal of neuroscience : the official journal of the Society for Neuroscience. 17:5046-5061.

Duque A, Spector R. 2019. A balanced evaluation of the evidence for adult neurogenesis in humans: implication for neuropsychiatric disorders. Brain structure & function. 224:2281-2295.

Ellis JK, Sorrells SF, Mikhailova S, Chavali M, Chang S, Sabeur K, McQuillen P, Rowitch DH. 2019. Ferret brain possesses young interneuron collections equivalent to human postnatal migratory streams. The Journal of comparative neurology.

Fujioka T, Kaneko N, Ajioka I, Nakaguchi K, Omata T, Ohba H, Fassler R, Garcia-Verdugo JM, Sekiguchi K, Matsukawa N, Sawamoto K. 2017. beta1 integrin signaling promotes neuronal migration along vascular scaffolds in the post-stroke brain. EBioMedicine. 16:195-203.

Garcia-Marques J, De Carlos JA, Greer CA, Lopez-Mascaraque L. 2010. Different astroglia permissivity controls the migration of olfactory bulb interneuron precursors. Glia. 58:218-230.

Garcia-Moreno F, Vasistha NA, Trevia N, Bourne JA, Molnar Z. 2012. Compartmentalization of cerebral cortical germinal zones in a lissencephalic primate and gyrencephalic rodent. Cerebral cortex. 22:482-492.

Geschwind DH, Rakic P. 2013. Cortical evolution: judge the brain by its cover. Neuron. 80:633-647.

Ghosh L, Jessberger S. 2013. Supersize me-new insights into cortical expansion and gyration of the mammalian brain. The EMBO journal. 32:1793-1795.
Gil-Perotin S, Duran-Moreno M, Belzunegui S, Luquin MR, Garcia-Verdugo JM. 2009. Ultrastructure of the subventricular zone in Macaca fascicularis and evidence of a mouse-like migratory stream. The Journal of comparative neurology. 514:533-554.
Hack MA, Saghatelyan A, de Chevigny A, Pfeifer A, Ashery-Padan R, Lledo PM, Gotz M. 2005. Neuronal fate determinants of adult olfactory bulb neurogenesis. Nature neuroscience. 8:865-872.
Hardy D, Malvaut S, Breton-Provencher V, Saghatelyan A. 2018. The role of calretinin-expressing granule cells in olfactory bulb functions and odor behavior. Scientific reports. 8:9385.
Homman-Ludiye J, Bourne JA. 2017. The marmoset: An emerging model to unravel the evolution and development of the primate neocortex. Developmental neurobiology. 77:263-272.
Ihrie RA, Alvarez-Buylla A. 2011. Lake-front property: a unique germinal niche by the lateral ventricles of the adult brain. Neuron. 70:674-686.
Ikeda M, Hirota Y, Sakaguchi M, Yamada O, Kida YS, Ogura T, Otsuka T, Okano H, Sawamoto K. 2010. Expression and proliferation-promoting role of Diversin in the neuronally committed precursor cells migrating in the adult mouse brain. Stem cells. 28:2017-2026.
Inta D, Alfonso J, von Engelhardt J, Kreuzberg MM, Meyer AH, van Hooft JA, Monyer H. 2008. Neurogenesis and widespread forebrain migration of distinct GABAergic neurons from the postnatal subventricular zone. Proceedings of the National Academy of Sciences of the United States of America. 105:20994-20999.
Jankovski A, Sotelo C. 1996. Subventricular zone-olfactory bulb migratory pathway in the adult mouse: cellular composition and specificity as determined by heterochronic and heterotopic transplantation. The Journal of comparative neurology. 371:376-396.
Jinnou H, Sawada M, Kawase K, Kaneko N, Herranz-Perez V, Miyamoto T, Kawaue T, Miyata T, Tabata Y, Akaike T, Garcia-Verdugo JM, Ajioka I, Saitoh S, Sawamoto K. 2018. Radial Glial Fibers Promote Neuronal Migration and Functional Recovery after Neonatal Brain Injury. Cell stem cell. 22:128-137 e129.
Kaneko N, Herranz-Perez V, Otsuka T, Sano H, Ohno N, Omata T, Nguyen HB, Thai TQ, Nambu A, Kawaguchi Y, Garcia-Verdugo JM, Sawamoto K. 2018. New neurons use Slit-Robo signaling to migrate through the glial meshwork and approach a lesion for functional regeneration. Science advances. 4:eaav0618.
Kaneko N, Marin O, Koike M, Hirota Y, Uchiyama Y, Wu JY, Lu Q, Tessier-Lavigne M, Alvarez-Buylla A, Okano H, Rubenstein JL, Sawamoto K. 2010. New neurons clear the path of astrocytic processes for their rapid migration in the adult brain. Neuron. 67:213-223.
Kaneko N, Sawada M, Sawamoto K. 2017. Mechanisms of neuronal migration in the adult brain. Journal of neurochemistry. 141:835-847.

Kato Y, Kaneko N, Sawada M, Ito K, Arakawa S, Murakami S, Sawamoto K. 2012. A subtype-specific critical period for neurogenesis in the postnatal development of mouse olfactory glomeruli. PloS one. 7:e48431.

Kelava I, Reillo I, Murayama AY, Kalinka AT, Stenzel D, Tomancak P, Matsuzaki F, Lebrand C, Sasaki E, Schwamborn JC, Okano H, Huttner WB, Borrell V. 2012. Abundant occurrence of basal radial glia in the subventricular zone of embryonic neocortex of a lissencephalic primate, the common marmoset Callithrix jacchus. Cerebral cortex. 22:469-481.

Kempermann G, Gast D, Kronenberg G, Yamaguchi M, Gage FH. 2003. Early determination and long-term persistence of adult-generated new neurons in the hippocampus of mice. Development. 130:391-399.

Kohler SJ, Williams NI, Stanton GB, Cameron JL, Greenough WT. 2011. Maturation time of new granule cells in the dentate gyrus of adult macaque monkeys exceeds six months. Proceedings of the National Academy of Sciences of the United States of America. 108:10326-10331.

Kojima T, Hirota Y, Ema M, Takahashi S, Miyoshi I, Okano H, Sawamoto K. 2010. Subventricular zone-derived neural progenitor cells migrate along a blood vessel scaffold toward the post-stroke striatum. Stem cells. 28:545-554.

Kornack DR, Rakic P. 2001. The generation, migration, and differentiation of olfactory neurons in the adult primate brain. Proceedings of the National Academy of Sciences of the United States of America. 98:4752-4757.

Kosaka T, Kosaka K. 2016. Neuronal organization of the main olfactory bulb revisited. Anatomical science international. 91:115-127.

Le Magueresse C, Alfonso J, Khodosevich K, Arroyo Martin AA, Bark C, Monyer H. 2011. "Small axonless neurons": postnatally generated neocortical interneurons with delayed functional maturation. The Journal of neuroscience : the official journal of the Society for Neuroscience. 31:16731-16747.

Lemasson M, Saghatelyan A, Olivo-Marin JC, Lledo PM. 2005. Neonatal and adult neurogenesis provide two distinct populations of newborn neurons to the mouse olfactory bulb. The Journal of neuroscience : the official journal of the Society for Neuroscience. 25:6816-6825.

Leuner B, Kozorovitskiy Y, Gross CG, Gould E. 2007. Diminished adult neurogenesis in the marmoset brain precedes old age. Proceedings of the National Academy of Sciences of the United States of America. 104:17169-17173.

Lim DA, Alvarez-Buylla A. 2016. The Adult Ventricular-Subventricular Zone (V-SVZ) and Olfactory Bulb (OB) Neurogenesis. Cold Spring Harbor perspectives in biology. 8.

Lim L, Mi D, Llorca A, Marin O. 2018. Development and Functional Diversification of Cortical Interneurons. Neuron. 100:294-313.

Lindvall O, Kokaia Z. 2015. Neurogenesis following Stroke Affecting the Adult Brain. Cold Spring Harbor perspectives in biology. 7.

Lledo PM, Valley M. 2016. Adult Olfactory Bulb Neurogenesis. Cold Spring Harbor perspectives in biology. 8.

Lois C, Alvarez-Buylla A. 1994. Long-distance neuronal migration in the adult mammalian brain. Science. 264:1145-1148.

Lois C, Garcia-Verdugo JM, Alvarez-Buylla A. 1996. Chain migration of neuronal precursors. Science. 271:978-981.

Mathews EA, Morgenstern NA, Piatti VC, Zhao C, Jessberger S, Schinder AF, Gage FH. 2010. A distinctive layering pattern of mouse dentate granule cells is generated by developmental and adult neurogenesis. The Journal of comparative neurology. 518:4479-4490.

Mathis C, Schroter A, Thallmair M, Schwab ME. 2010. Nogo-a regulates neural precursor migration in the embryonic mouse cortex. Cerebral cortex. 20:2380-2390.

Merkle FT, Fuentealba LC, Sanders TA, Magno L, Kessaris N, Alvarez-Buylla A. 2014. Adult neural stem cells in distinct microdomains generate previously unknown interneuron types. Nature neuroscience. 17:207-214.

Merkle FT, Mirzadeh Z, Alvarez-Buylla A. 2007. Mosaic organization of neural stem cells in the adult brain. Science. 317:381-384.

Mirzadeh Z, Merkle FT, Soriano-Navarro M, Garcia-Verdugo JM, Alvarez-Buylla A. 2008. Neural stem cells confer unique pinwheel architecture to the ventricular surface in neurogenic regions of the adult brain. Cell stem cell. 3:265-278.

Molnar Z, Clowry GJ, Sestan N, Alzu'bi A, Bakken T, Hevner RF, Huppi PS, Kostovic I, Rakic P, Anton ES, Edwards D, Garcez P, Hoerder-Suabedissen A, Kriegstein A. 2019. New insights into the development of the human cerebral cortex. Journal of anatomy. 235:432-451.

Paredes MF, James D, Gil-Perotin S, Kim H, Cotter JA, Ng C, Sandoval K, Rowitch DH, Xu D, McQuillen PS, Garcia-Verdugo JM, Huang EJ, Alvarez-Buylla A. 2016. Extensive migration of young neurons into the infant human frontal lobe. Science. 354.

Paredes MF, Sorrells SF, Cebrian-Silla A, Sandoval K, Qi D, Kelley KW, James D, Mayer S, Chang J, Auguste KI, Chang EF, Gutierrez Martin AJ, Kriegstein AR, Mathern GW, Oldham MC, Huang EJ, Garcia-Verdugo JM, Yang Z, Alvarez-Buylla A. 2018. Does Adult Neurogenesis Persist in the Human Hippocampus? Cell stem cell. 23:780-781.

Parolisi R, Cozzi B, Bonfanti L. 2018. Humans and Dolphins: Decline and Fall of Adult Neurogenesis. Frontiers in neuroscience. 12:497.

Pencea V, Bingaman KD, Freedman LJ, Luskin MB. 2001. Neurogenesis in the subventricular zone and rostral migratory stream of the neonatal and adult primate forebrain. Experimental neurology. 172:1-16.

Petreanu L, Alvarez-Buylla A. 2002. Maturation and death of adult-born olfactory bulb granule neurons: role of olfaction. The Journal of neuroscience : the official journal of the Society for Neuroscience. 22:6106-6113.

Quinones-Hinojosa A, Sanai N, Soriano-Navarro M, Gonzalez-Perez O, Mirzadeh Z, Gil-Perotin S, Romero-Rodriguez R, Berger MS, Garcia-Verdugo JM, Alvarez-Buylla A. 2006. Cellular composition and cytoarchitecture of the adult human subventricular zone: a niche of neural stem cells. The Journal of comparative neurology. 494:415-434.

Rakic P. 2009. Evolution of the neocortex: a perspective from developmental biology. Nature reviews Neuroscience. 10:724-735.
Sakamoto M, Kageyama R, Imayoshi I. 2014. The functional significance of newly born neurons integrated into olfactory bulb circuits. Frontiers in neuroscience. 8:121.
Sanai N, Nguyen T, Ihrie RA, Mirzadeh Z, Tsai HH, Wong M, Gupta N, Berger MS, Huang E, Garcia-Verdugo JM, Rowitch DH, Alvarez-Buylla A. 2011. Corridors of migrating neurons in the human brain and their decline during infancy. Nature. 478:382-386.
Sanai N, Tramontin AD, Quinones-Hinojosa A, Barbaro NM, Gupta N, Kunwar S, Lawton MT, McDermott MW, Parsa AT, Manuel-Garcia Verdugo J, Berger MS, Alvarez-Buylla A. 2004. Unique astrocyte ribbon in adult human brain contains neural stem cells but lacks chain migration. Nature. 427:740-744.
Sawamoto K, Hirota Y, Alfaro-Cervello C, Soriano-Navarro M, He X, Hayakawa-Yano Y, Yamada M, Hikishima K, Tabata H, Iwanami A, Nakajima K, Toyama Y, Itoh T, Alvarez-Buylla A, Garcia-Verdugo JM, Okano H. 2011. Cellular composition and organization of the subventricular zone and rostral migratory stream in the adult and neonatal common marmoset brain. The Journal of comparative neurology. 519:690-713.
Schwab ME. 2010. Functions of Nogo proteins and their receptors in the nervous system. Nature reviews Neuroscience. 11:799-811.
Silva CG, Peyre E, Nguyen L. 2019. Cell migration promotes dynamic cellular interactions to control cerebral cortex morphogenesis. Nature reviews Neuroscience. 20:318-329.
Snapyan M, Lemasson M, Brill MS, Blais M, Massouh M, Ninkovic J, Gravel C, Berthod F, Gotz M, Barker PA, Parent A, Saghatelyan A. 2009. Vasculature guides migrating neuronal precursors in the adult mammalian forebrain via brain-derived neurotrophic factor signaling. The Journal of neuroscience : the official journal of the Society for Neuroscience. 29:4172-4188.
Sorrells SF, Paredes MF, Cebrian-Silla A, Sandoval K, Qi D, Kelley KW, James D, Mayer S, Chang J, Auguste KI, Chang EF, Gutierrez AJ, Kriegstein AR, Mathern GW, Oldham MC, Huang EJ, Garcia-Verdugo JM, Yang Z, Alvarez-Buylla A. 2018. Human hippocampal neurogenesis drops sharply in children to undetectable levels in adults. Nature. 555:377-381.
Wackermannova M, Pinc L, Jebavy L. 2016. Olfactory sensitivity in mammalian species. Physiological research. 65:369-390.
Wang C, Liu F, Liu YY, Zhao CH, You Y, Wang L, Zhang J, Wei B, Ma T, Zhang Q, Zhang Y, Chen R, Song H, Yang Z. 2011. Identification and characterization of neuroblasts in the subventricular zone and rostral migratory stream of the adult human brain. Cell research. 21:1534-1550.
Yamaguchi M, Mori K. 2005. Critical period for sensory experience-dependent survival of newly generated granule cells in the adult mouse olfactory bulb. Proceedings of the National Academy of Sciences of the United States of America. 102:9697-9702.
Yamashita T, Ninomiya M, Hernandez Acosta P, Garcia-Verdugo JM, Sunabori T, Sakaguchi M, Adachi K, Kojima T, Hirota Y, Kawase T, Araki N, Abe K, Okano H, Sawamoto K. 2006. Subventricular zone-derived neuroblasts migrate and differentiate into mature

neurons in the post-stroke adult striatum. The Journal of neuroscience : the official journal of the Society for Neuroscience. 26:6627-6636.
Young KM, Fogarty M, Kessaris N, Richardson WD. 2007. Subventricular zone stem cells are heterogeneous with respect to their embryonic origins and neurogenic fates in the adult olfactory bulb. The Journal of neuroscience : the official journal of the Society for Neuroscience. 27:8286-8296.
Yu S, Shu H, Yang T, Huang H, Li S, Zhao Z, Kuang Y. 2016. Upregulated expression of Nogo-A and NgR in an experimental model of focal microgyria regulates the migration, proliferation and self-renewal of subventricular zone neural progenitors. Biochemical and biophysical research communications. 473:482-489.
Zhang K, Sejnowski TJ. 2000. A universal scaling law between gray matter and white matter of cerebral cortex. Proceedings of the National Academy of Sciences of the United States of America. 97:5621-5626.

Figure legends

Figure 1: Organization of the V-SVZ at 0 and 1 month

A-C: Sagittal and coronal views of a common marmoset brain. In the illustration of sagittal view, different rostro-caudal levels from level I to level V are indicated (A). In the illustration of the coronal view (A'), coronal sections immunostained for DCX (B), and a coronal semi-thin section stained with toluidine blue for electron microscopy (C), subregions of the V-SVZ are indicated with different colors (LW: cyan broken lines, DW-collapsed: pink line, DW-open: pink broken line, EX: red lines).

D-F: Electron microscopy images of the LW at ages 0 months (D) and 1 month (E,F). Neuroblasts and astrocytes are indicated with pink and blue, respectively (F).

G-K: Electron microscopy images of the DW-open at 1 month. In the dorsal wall associated with corpus callosum (CC side), ependymal layers, but not the other layers, are distinguishable (G). In the striatal side (St side) of the DW-open (H,I), neuroblasts, astrocytes, ependymal cells, and microglia are indicated by pink, blue, green and brown, respectively (I). In a chain, neuroblasts (Nb) make a small adherens junction (filled arrowheads) and free spaces (open arrowheads) between them (J, inset shows higher magnification image of the boxed area). Higher magnification image of the boxed area in (I) shows a neuroblast (Nb) integrated into a chain contacting an astrocytic (As) cell body (blue arrowheads) (K).

L-N: Electron microscopy images of putative neural stem cells (type B1 cells) in the St side of the DW-open at 1 month. Type B1 cell (cyan) displays radial morphology and presents an

apical expansion that contacts the lateral ventricle (L, filled arrowheads) and a basal expansion containing many intermediate filaments (L, open arrowheads). M and N show higher magnification images of the boxed area in L. The filled arrow in M indicates the primary cilium, with abundant pericentriolar material, and the open arrow in N indicates a bundle of intermediate filaments.

O-R: Electron microscopy images of the EX. In the EX (O), the higher magnification image of a large chain of neuroblasts (the boxed area) shows neuroblasts, astrocytes, microglia, and non-myelinated axons (pink, blue, brown and yellow, respectively) surrounding the chain (P). In a chain, neuroblasts (Nb) make a small adherens junction (filled arrowheads) and free spaces (open arrowheads) between them (Q, inset shows a higher magnification image of the boxed area). Higher magnification image of the boxed area in (P) shows an individual neuroblast (Nb) migrating into the corpus callosum contacting non-myelinated axons (yellow arrowheads) (R).

Scale bars: 500 μm, B, C; 100 μm, D, E, G, H, O; 5 μm, F, I, L, P; 0.5 μm, J, K, Q, R; 0.2 μm, M, N

LW: lateral wall, DW: dorsolateral wall, EX: extension, EL: ependymal cell layer, HG: hypocellular gap, RL: ribbon layer.

Figure 2: Quantification of neuroblasts in the V-SVZ at 1, 4, 6 and 30 months

A: An illustration of V-SVZ in a coronal brain section at level III indicating the V-SVZ subregions and the areas shown in C-D.

B: The number of DCX+ neuroblasts in the V-SVZ at 1, 4 and 6 months.

C-F: Coronal sections of the V-SVZ immunostained for DCX. The DCX+ neuroblasts distributed in the LW (C) are gradually reduced with age by 6 months, and very few remain in adulthood. Neuroblasts are densely distributed in the EX at 1 month, but sharply decline by 6 months, and completely disappear in adulthood (30 months)(D, E). Neuroblasts in the DW-open decline in number with age, but contain small chains of DCX+ cells even in adulthood (F). Nuclei were stained with Hoechst 33342. C-E: single z-axis images, F: z-stack projection images.

Scale bars: 100 μm, D; 20 μm, C,E,F

LW: lateral wall (cyan broken lines), DW: dorsolateral wall (pink lines), EX: extension (red lines)

The quantification data are presented as mean ± SEM, $*P<0.05$

Figure 3: Neuroblast migration toward the olfactory bulb and neocortex at 1, 4 and 6 months

A-A": Schematic illustration of a common marmoset brain. The sagittal view (A) indicates the RMS (blue line) and the rostrocaudal levels of the coronal views (A'-A"). In the coronal views, the areas for image acquisition and histological analyses are indicated with boxes and broken lines (A', A") (LW: cyan lines, EX: red lines).

B-C: Distribution of DCX+ neuroblasts in the RMS at 1, 4, and 6 months of age. The confocal images show transverse sections of the olfactory tract immunostained for DCX (B).

Higher magnification images of the RMS (boxed areas) are shown in the panels below. Nuclei were stained with Hoechst 33342. The graph shows the density of DCX+ neuroblasts in the RMS at 1, 4 and 6 months (C).

D-K: Distribution of DCX+ neuroblasts in the corpus callosum (CC) and the neocortex (Ncx) at 1, 4, and 6 months of age. The images show DCX+ neuroblasts close to CD31+ blood vessels in the deeper layer Ncx at 1 month (D) and 4 months (E), at the boundary between the V-SVZ extension (EX) and CC (F, arrowheads indicate DCX+ cells directed radially toward Ncx) at 1 month, and in the upper layer Ncx at 1 month (G) and 4 months (H) (D,E,G,H: z-stack projection images, F: single z-axis image). Nuclei were stained with Hoechst 33342. The graphs show the density of DCX+ cells distributed in the CC-Ncx at 1, 4 and 6 months (I) and the percentage of these cells in each migration mode (J, chain formation and contact with blood vessels) at 1 month and 4 months. Confocal images of the CC and cortical white matter immunostained for DCX and myelin marker MBP at 1 month and 4 months show progressive myelination (K). Higher magnification images of the boxed area are shown below.

L: Proliferation of neuroblasts in different regions and at different ages. In confocal images, DCX+ cells in 1-month RMS, but not in the Ncx or 6-month St, were occasionally colabeled with proliferation marker Ki67 (arrowheads).

Scale bars: 500 μm, K top; 100 μm, B top; 50 μm, K bottom; 20 μm, B bottom; 10 μm, D-H, L

The quantification data are presented as mean ± SEM, *P<0.05, **P<0.01

Figure 4: Comparison of cell proliferation activities among the V-SVZ subregion at 0, 1, 4, and 6 months

A-C: Common marmoset V-SVZ (level III) immunostained for Ki67. Cell nuclei were stained with Hoechst 33342. Z-stack images show Ki67+ proliferating cells in the LW (A) and the EX (B) at 0, 1, 6 and 30 months. Confocal images of the EX immunostained for Ki67 and a transit amplifying neuronal progenitor marker, Mash1, show a large cluster of Ki67+Mash1+ cells at 1 month, but not at 6 months (C).

D-E: Number of Ki67+ cells at 0, 1, 4, and 6 months of age (D) and Ki67+Mash1+ cells at 0, 1, and 4 months of age (E) in the LW, DW and EX.

F-H: Density of Ki67+Mash1+ cells in the LW, DW and EX at 0 months (F), 1 month (G), and 4 months (H).

Scale bars: 200 μm, B; 20 μm, A; 10 μm, C

LW: lateral wall, DW: dorsolateral wall, EX: extension

The quantification data are presented as mean ± SEM, $*P<0.05$, $**P<0.01$

Figure 5: Fates of the postnatally born cells depending on their birthdate and destination

A: Experimental designs showing timings of BrdU and/or EdU injections to label neonatal-born cells (red) and 1-month-born cells (magenta) in common marmosets during postnatal development.

B: Low magnification image of a whole olfactory bulb (OB) immunostained for a mature neuronal marker, NeuN. Higher magnification image of the boxed area presented below shows layer organization (inner granule cell layer: iGCL, outer GCL: oGCL, and glomerular layer: GL).

C-D: Short-term fate of postnatally born cells in the OB. EdU-labeled neonatal-born and 1-month-born DCX+ cells in 1-month (C) and 2-month (D) OB, respectively.

E-K: Long-term fate of neonatal-born (BrdU+) and 1-month-born (EdU+) neurons in the OB. BrdU+ and EdU+ cells did not express DCX (E), but expressed NeuN (F) in 4-month and 6-month GCL. The graphs show the density of NeuN+ cells labeled with BrdU or EdU in the whole OB (G) at 4 and 6 months and the percentage of their distribution in each cell layer of the GCL (H) and the GL (I) at 6 months. Confocal images (J) and the percentage of interneuron subtype marker calretinin (CR) expression in BrdU+ and EdU+ cells (K).

L-P: Short-term fate of postnatally born cells in the corpus callosum (CC) and neocortex (Ncx). EdU-labeled neonatal-born and 1-month-born DCX+ cells in the 1-month (L) and 2-month deeper layer Ncx (M), respectively. The graphs show the density of EdU+DCX+ cells in the CC-Ncx (N), the percentage of EdU-labeled cells among all the DCX+ cells distributed in the V-SVZ extension (EX) and the CC-Ncx (O), and the translocation index of the EdU+DCX+ cells (P).

Q-U: Long-term fate of neonatal-born (BrdU+) and 1-month-born (EdU+) cells in the Ncx. Z-stack projection images show BrdU+ (Q) and EdU+ (R) cells expressing DCX in the 6-month Ncx. Confocal image shows a BrdU+NeuN+ cell and its x-z and y-z plane views (S).

The graphs show density of the DCX+ cells labeled with BrdU or EdU in 4-month and 6-month Ncx (T), and the percentage of their distribution in the deeper layer (layer V-VI) Ncx at 6 months (U).

Scale bars: 200 μm, B; 5 μm, C-F, J, L-M, Q-S

The quantification data are presented as mean ± SEM, *P<0.05

Figure 6: Postnatal neurogenesis in the common marmoset dentate gyrus

A-B: Cell proliferation in the postnatal subgranular zone (SGZ) of the dentate gyrus (DG). Confocal images (A, left, 0 months, right, 1 month) and the number (B) of Ki67+ cells distributed in the SGZ of 0-month and 1-month animals.

C: Confocal images of neonatal-born and 1-month-born EdU+cells in the DG immunostained for DCX and NeuN at 1 and 2 months, respectively. The boundaries of the granule cell layer (GCL) are indicated with yellow broken lines.

D-F: Long-term fate of neonatal-born (BrdU+) and 1-month-born (EdU+) neurons in the DG. BrdU+ and EdU+ cells expressing NeuN (red and magenta arrowheads, respectively) were distributed in the hilus, SGZ, inner granule cell layer (iGCL), medial GCL (mGCL), and outer GCL (oGCL) in the 6-month DG (D). Higher magnification confocal images of a BrdU+NeuN+ cell (E) and EdU+NeuN+ cells (E**'**) in the GCL, and BrdU+NeuN+ cell in the SGZ (F) are presented. The graphs show the density of BrdU+NeuN+ cells and EdU+NeuN+ cells (**G**) and the percentage of these cells' distribution in each layer (**H**) of the DG at 6 months.

Scale bars: 50 μm, C, D; 20 μm, A, F; 5 μm, E, E’

The quantification data are presented as mean ± SEM, *P<0.05

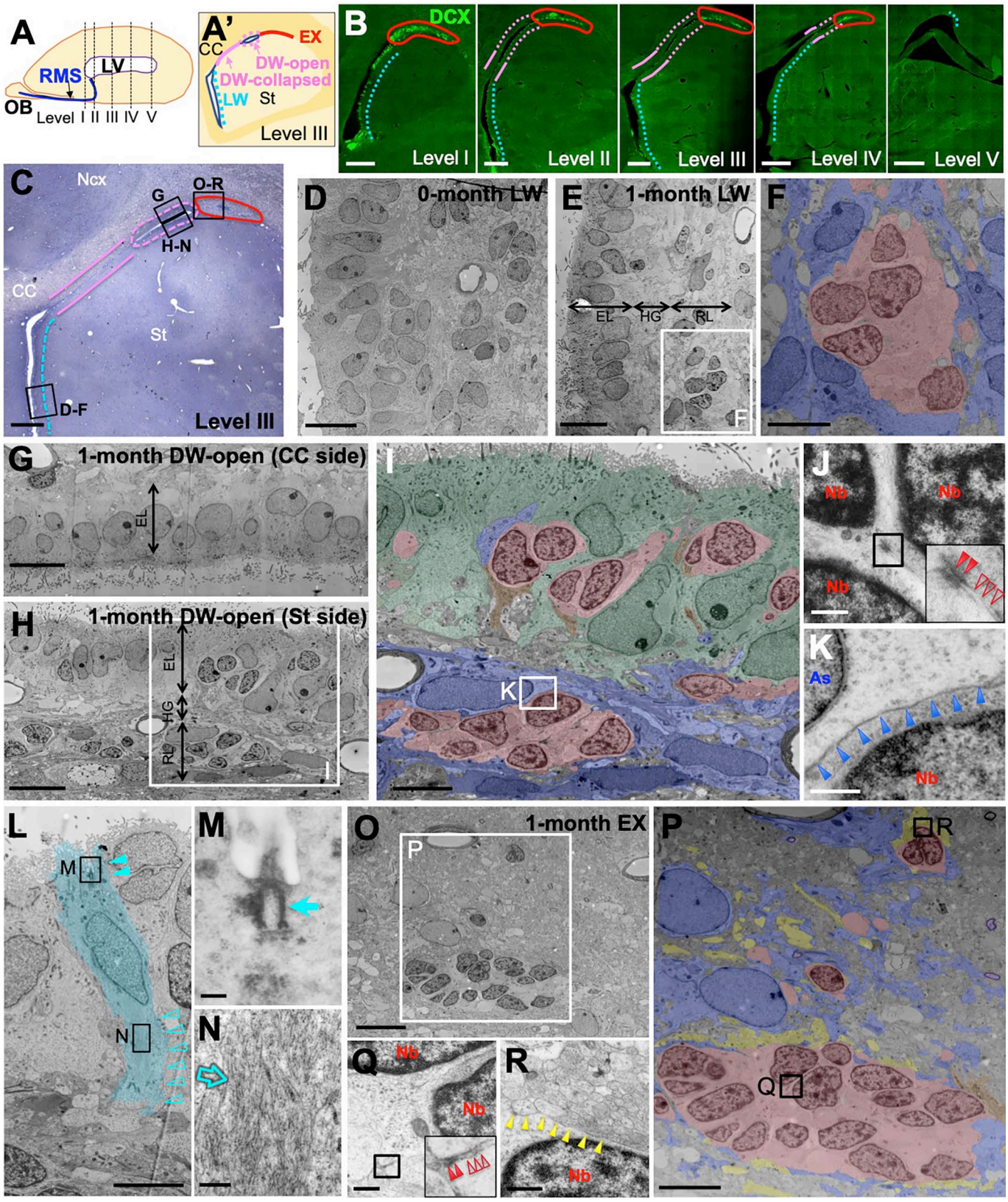
A
RMS
LV
OB
Level I II III IV V
A'
CC
EX
DW-open
DW-collapsed
LW
St
Level III
B
DCX
Level I
Level II
Level III
Level IV
Level V
C
Ncx
G
O-R
H-N
CC
St
D-F
Level III
D
0-month LW
E
1-month LW
EL
HG
RL
F
F
G
1-month DW-open (CC side)
EL
H
1-month DW-open (St side)
EL
HG
RL
I
I
K
J
Nb
Nb
Nb
K
As
Nb
L
M
N
M
N
O
1-month EX
P
P
R
Q
Q
Nb
Nb
R
Nb

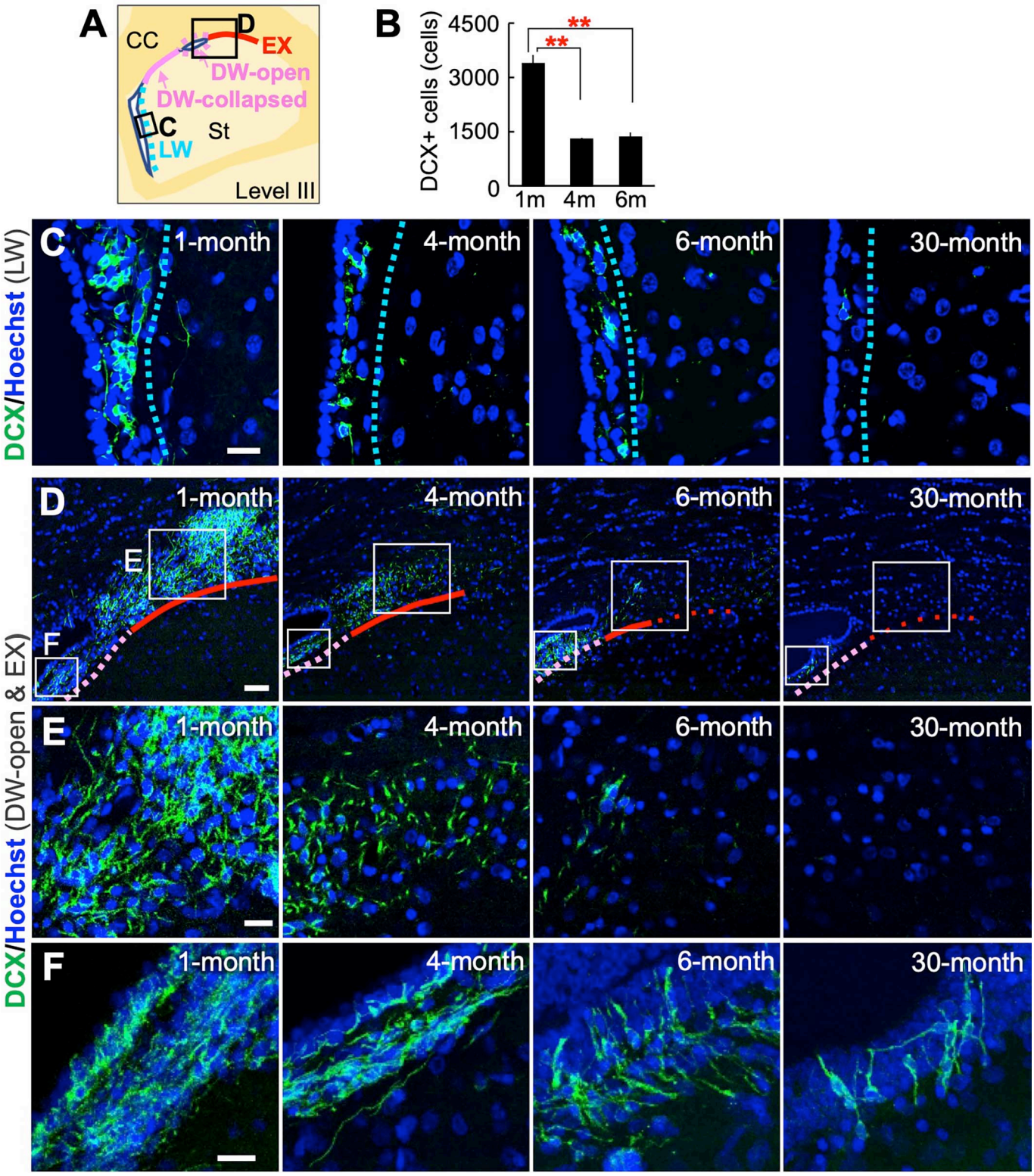
A
CC
D
EX
DW-open
DW-collapsed
C
St
LW
Level III
B
DCX+ cells (cells)
4500
3000
1500
0
**
**
1m
4m
6m
DCX/Hoechst (LW)
C
1-month
4-month
6-month
30-month
DCX/Hoechst (DW-open & EX)
D
E
F
1-month
4-month
6-month
30-month

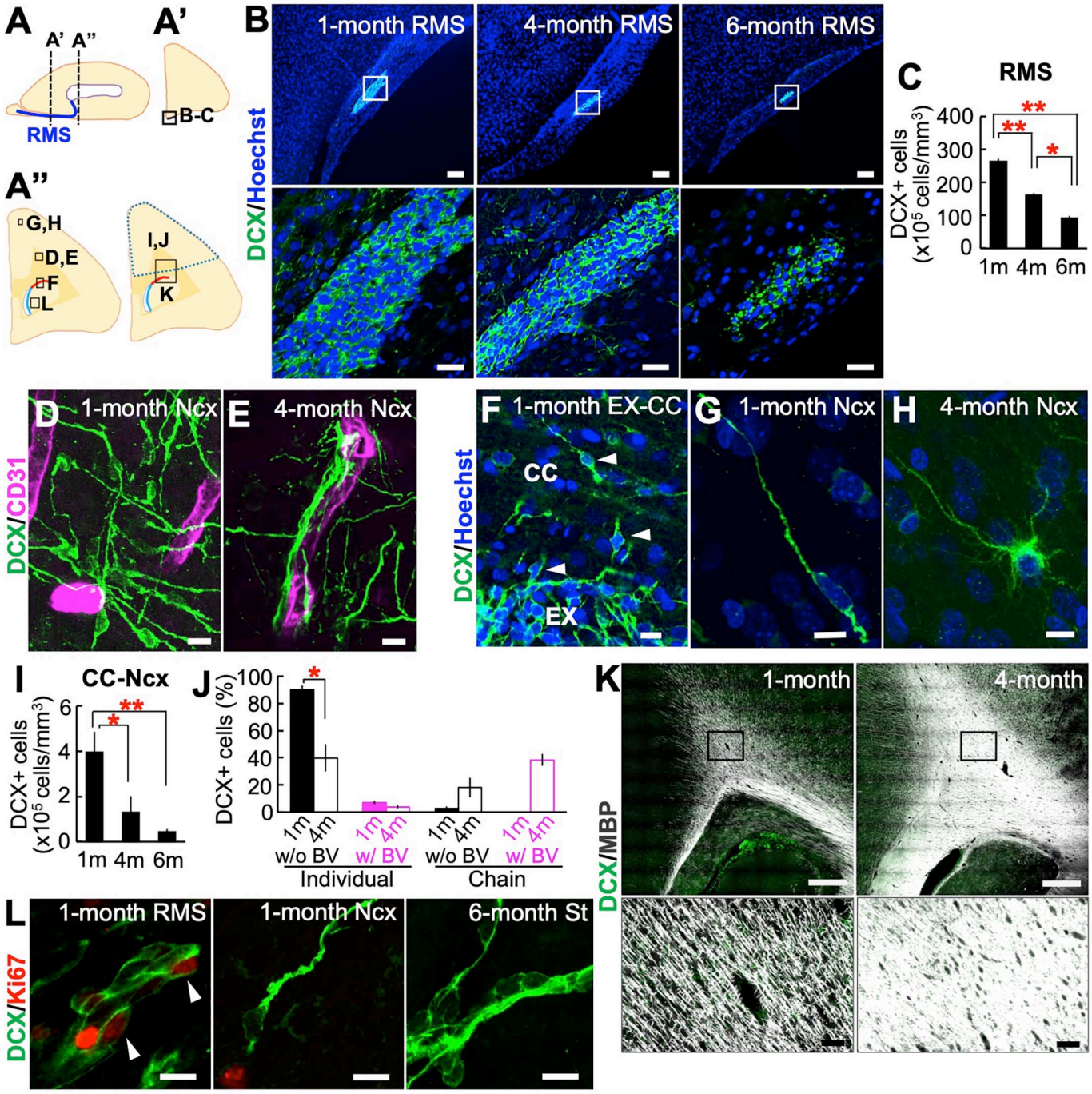
A
A' A"
RMS
A'
B-C
A"
G,H
D,E
F
L
I,J
K
B
1-month RMS
4-month RMS
6-month RMS
DCX/Hoechst
C
RMS
DCX+ cells
(x10^5 cells/mm^3)
400
300
200
100
0
1m 4m 6m
**
**
*
D
1-month Ncx
E
4-month Ncx
DCX/CD31
F
1-month EX-CC
CC
EX
DCX/Hoechst
G
1-month Ncx
H
4-month Ncx
I
CC-Ncx
DCX+ cells
(x10^5 cells/mm^3)
6
4
2
0
1m 4m 6m
**
*
J
DCX+ cells (%)
100
80
60
40
20
0
*
1m 4m 1m 4m 1m 4m 1m 4m
w/o BV w/ BV w/o BV w/ BV
Individual
Chain
K
1-month
4-month
DCX/MBP
L
1-month RMS
1-month Ncx
6-month St
DCX/Ki67

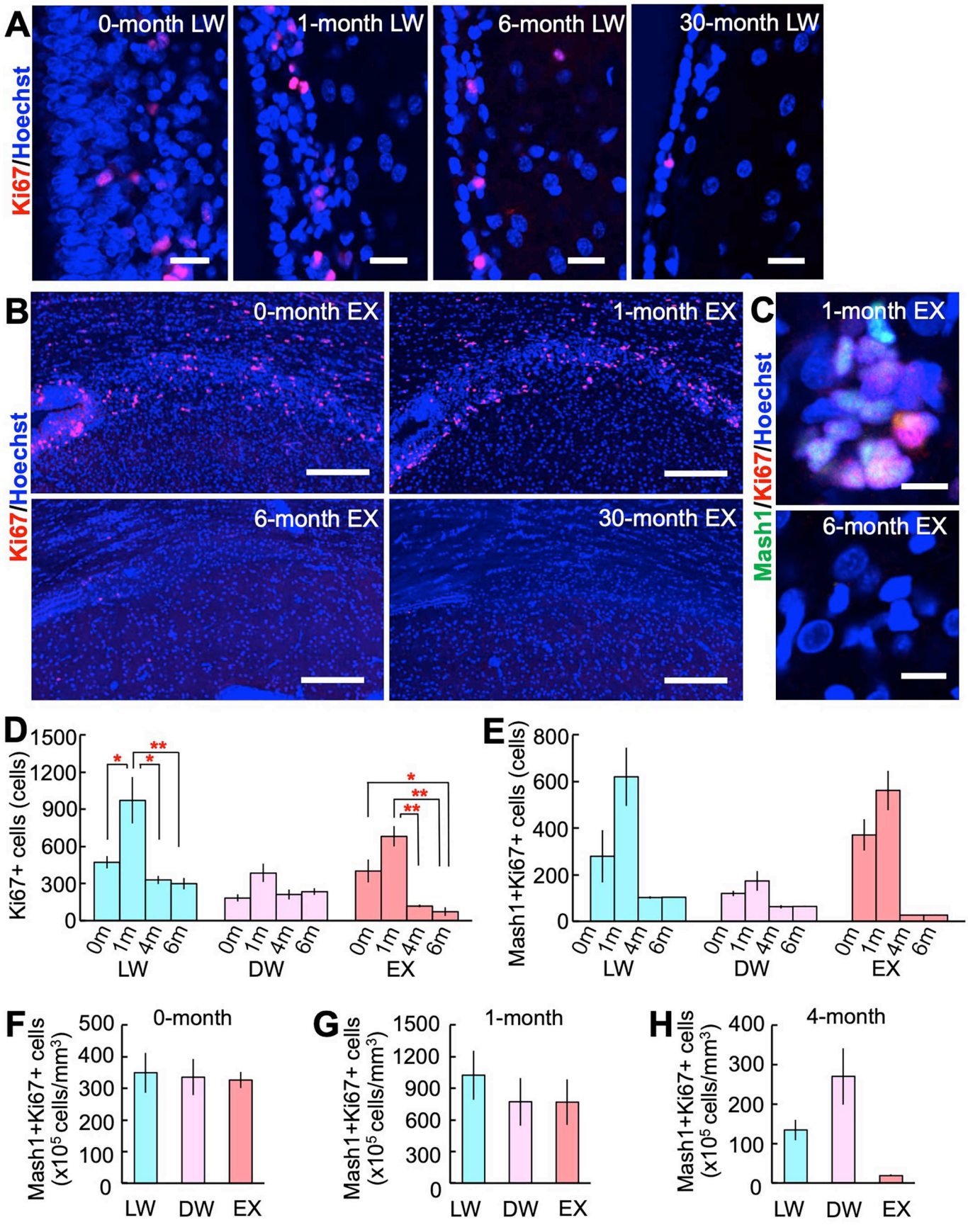
A
0-month LW
1-month LW
6-month LW
30-month LW
Ki67/Hoechst
B
0-month EX
1-month EX
6-month EX
30-month EX
Ki67/Hoechst
C
1-month EX
6-month EX
Mash1/Ki67/Hoechst
D
Ki67+ cells (cells)
1500
1200
900
600
300
0
0m 1m 4m 6m
LW
DW
EX
E
Mash1+Ki67+ cells (cells)
800
600
400
200
0
F
0-month
Mash1+Ki67+ cells (x10^5 cells/mm^3)
500
400
300
200
100
0
LW DW EX
G
1-month
1500
1200
900
600
300
0
H
4-month
400
300
200
100
0

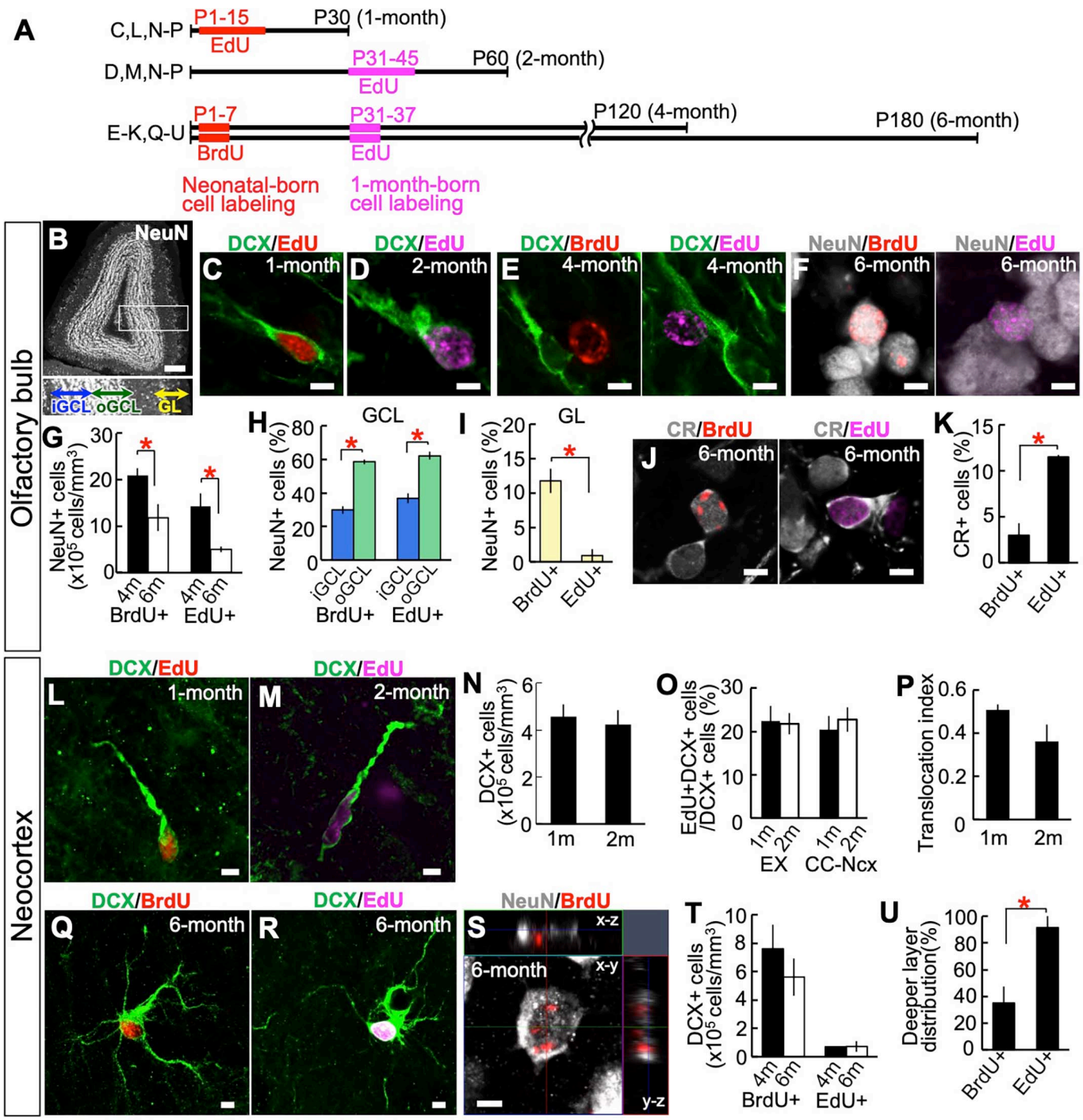
A
C,L,N-P
P1-15
EdU
P30 (1-month)
D,M,N-P
P31-45
EdU
P60 (2-month)
E-K,Q-U
P1-7
BrdU
P31-37
EdU
P120 (4-month)
P180 (6-month)
Neonatal-born cell labeling
1-month-born cell labeling
Olfactory bulb
B NeuN
iGCL oGCL GL
DCX/EdU
C 1-month
DCX/EdU
D 2-month
DCX/BrdU
E 4-month
DCX/EdU
4-month
NeuN/BrdU
F 6-month
NeuN/EdU
6-month
G
NeuN+ cells (x10^5 cells/mm^3)
4m 6m 4m 6m
BrdU+ EdU+
H
GCL
NeuN+ cells (%)
iGCL oGCL iGCL oGCL
BrdU+ EdU+
I
GL
NeuN+ cells (%)
BrdU+ EdU+
CR/BrdU
J 6-month
CR/EdU
6-month
K
CR+ cells (%)
BrdU+ EdU+
Neocortex
DCX/EdU
L 1-month
DCX/EdU
M 2-month
N
DCX+ cells (x10^5 cells/mm^3)
1m 2m
O
EdU+DCX+ cells /DCX+ cells (%)
1m 2m 1m 2m
EX CC-Ncx
P
Translocation index
1m 2m
DCX/BrdU
Q 6-month
DCX/EdU
R 6-month
NeuN/BrdU
S x-z
6-month x-y
y-z
T
DCX+ cells (x10^5 cells/mm^3)
4m 6m 4m 6m
BrdU+ EdU+
U
Deeper layer distribution(%)
BrdU+ EdU+

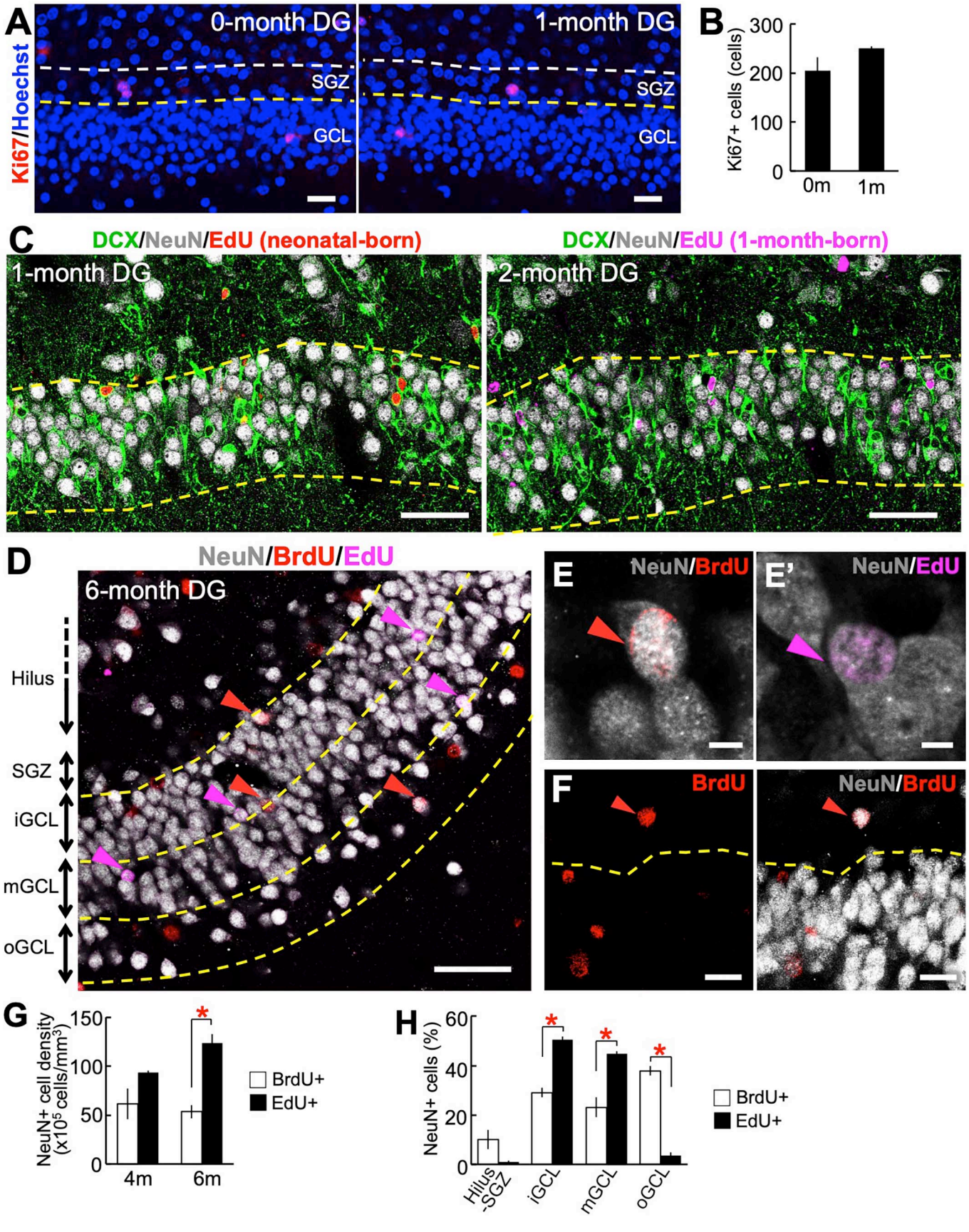
A
Ki67/Hoechst
0-month DG
1-month DG
SGZ
GCL
B
Ki67+ cells (cells)
300
200
100
0
0m
1m
C
DCX/NeuN/EdU (neonatal-born)
DCX/NeuN/EdU (1-month-born)
1-month DG
2-month DG
D
NeuN/BrdU/EdU
6-month DG
Hilus
SGZ
iGCL
mGCL
oGCL
E
NeuN/BrdU
E'
NeuN/EdU
F
BrdU
NeuN/BrdU
G
NeuN+ cell density (x10^5 cells/mm^3)
150
100
50
0
4m
6m
BrdU+
EdU+
H
NeuN+ cells (%)
60
40
20
0
Hilus -SGZ
iGCL
mGCL
oGCL
BrdU+
EdU+